

# Parameterizations of US wildfire and prescribed fire emission ratios and emission factors based on FIREX-AQ aircraft measurements

Georgios I. Gkatzelis<sup>1,2,†</sup>, Matthew M. Coggon<sup>2</sup>, Chelsea E. Stockwell<sup>1,2</sup>, Rebecca S. Hornbrook<sup>3</sup>, Hannah Allen<sup>4</sup>, Eric C. Apel<sup>3</sup>, Megan M. Bela<sup>1,2,Δ</sup>, Donald R. Blake<sup>5</sup>, Ilann Bourgeois<sup>1,2,~</sup>, Steven S. Brown<sup>2,6</sup>, Pedro Campuzano-Jost<sup>1,6</sup>, Jason M. St. Clair<sup>7,8</sup>, James H. Crawford<sup>9</sup>, John D. Crounse<sup>10</sup>, Douglas A. Day<sup>1,6</sup>, Joshua P. DiGangi<sup>9</sup>, Glenn S. Diskin<sup>9</sup>, Alan Fried<sup>11</sup>, Jessica B. Gilman<sup>2</sup>, Hongyu Guo<sup>1,6</sup>, Johnathan W. Hair<sup>9</sup>, Hannah S. Halliday<sup>9,‡</sup>, Thomas F. Hanisco<sup>7</sup>, Reem Hannun<sup>7,12,·</sup>, Alan Hills<sup>3</sup>, L. Gregory Huey<sup>13</sup>, Jose L. Jimenez<sup>1,6</sup>, Joseph M. Katich<sup>1,2</sup>, Aaron Lamplugh<sup>1,2</sup>, Young Ro Lee<sup>13</sup>, Jin Liao<sup>7,14</sup>, Jakob Lindaas<sup>15,§</sup>, Stuart A. McKeen<sup>1,2</sup>, Tomas Mikoviny<sup>16</sup>, Benjamin A. Nault<sup>1,6,||,‘</sup>, J. Andrew Neuman<sup>1,2</sup>, John B. Nowak<sup>9</sup>, Demetrios Pagonis<sup>1,6,¶</sup>, Jeff Peischl<sup>1,2</sup>, Anne E. Perring<sup>1,17</sup>, Felix Piel<sup>16,18,19</sup>, Pamela S. Rickly<sup>1,2</sup>, Michael A. Robinson<sup>1,2,6</sup>, Andrew W. Rollins<sup>2</sup>, Thomas B. Ryerson<sup>2,^</sup>, Melinda K. Schueneman<sup>1,6</sup>, Rebecca H. Schwantes<sup>2</sup>, Joshua P. Schwarz<sup>2</sup>, Kanako Sekimoto<sup>20</sup>, Vanessa Selimovic<sup>21</sup>, Taylor Shingler<sup>9</sup>, David J. Tanner<sup>13</sup>, Laura Tomsche<sup>9,22,\*,#</sup>, Krystal T. Vasquez<sup>10</sup>, Patrick R. Veres<sup>2,∅</sup>, Rebecca Washenfelder<sup>2</sup>, Petter Weibring<sup>10</sup>, Paul O. Wennberg<sup>10,23</sup>, Armin Wisthaler<sup>16,18</sup>, Glenn M. Wolfe<sup>7</sup>, Caroline C. Womack<sup>1,2</sup>, Lu Xu<sup>10,+,x</sup>, Katherine Ball<sup>4</sup>, Robert J. Yokelson<sup>21</sup>, Carsten Warneke<sup>2</sup>

<sup>1</sup> Cooperative Institute for Research in Environmental Sciences, University of Colorado Boulder, Boulder, CO, USA

<sup>2</sup> NOAA Chemical Sciences Laboratory (CSL), Boulder, CO, USA

<sup>3</sup> Atmospheric Chemistry Observations & Modeling Laboratory, NCAR, Boulder, CO, USA

<sup>4</sup> Division of Chemistry and Chemical Engineering, California Institute of Technology, Pasadena, CA, USA

<sup>5</sup> Department of Chemistry, University of California, Irvine, CA, USA

<sup>6</sup> Department of Chemistry, University of Colorado Boulder, Boulder, CO, USA

<sup>7</sup> Atmospheric Chemistry and Dynamics Laboratory, NASA Goddard Space Flight Center, Greenbelt, MD, USA

<sup>8</sup> Joint Center for Earth Systems Technology, University of Maryland Baltimore County, Baltimore, MD, USA

<sup>9</sup> NASA Langley Research Center, Hampton, VA, USA

<sup>10</sup> Institute of Arctic and Alpine Research, University of Colorado, Boulder, CO, USA

<sup>11</sup> Institute of Arctic & Alpine Research, University of Colorado, Boulder, CO, USA

<sup>12</sup> Joint Center for Earth Systems Technology, University of Maryland Baltimore County, Baltimore, MD, USA

<sup>13</sup> School of Earth and Atmospheric Sciences, Georgia Institute of Technology, Atlanta, GA, USA

<sup>14</sup> Goddard Earth Sciences Technology and Research (GESTAR II), University of Maryland, Baltimore County, MD, USA

<sup>15</sup> Colorado State University, Department of Atmospheric Science, Fort Collins, CO, USA

<sup>16</sup> Department of Chemistry, University of Oslo, Oslo, Norway

<sup>17</sup> Department of Chemistry, Colgate University, Hamilton, NY, USA

<sup>18</sup> Institut für Ionenphysik und Angewandte Physik, Universität Innsbruck, Innsbruck, Austria

<sup>19</sup> IONICON Analytik GmbH, Innsbruck, Austria

<sup>20</sup> Graduate School of Nanobioscience, Yokohama City University, 22-2 Seto, Kanazawa-ku, Yokohama, Kanagawa, Japan

<sup>21</sup> Department of Chemistry and Biochemistry, University of Montana, Missoula, MT, USA

<sup>22</sup> Universities Space Research Association, Columbia, MD, USA

<sup>23</sup> Division of Engineering and Applied Science, California Institute of Technology, Pasadena, CA, USA

Currently at:

<sup>†</sup> Institute of Energy and Climate Research, IEK-8: Troposphere, Forschungszentrum Jülich GmbH, Jülich, Germany

<sup>‡</sup> U.S. Environmental Protection Agency, Research Triangle Park, NC, USA

<sup>·</sup> Department of Geology and Environmental Science, University of Pittsburgh, PA, USA

<sup>Δ</sup> Google

<sup>~</sup> Univ. Savoie Mont Blanc, INRAE, CARRTEL, Thonon-les-Bains, France

<sup>§</sup> AGI / AAAS Congressional Science Fellow

53 <sup>||</sup> Center for Aerosol and Cloud Chemistry, Aerodyne Research Inc., Billerica, MA, USA  
54 <sup>..</sup> Department of Environmental Health and Engineering, Johns Hopkins University, MD, USA  
55 <sup>¶</sup> Weber State University, Ogden, UT, USA  
56 <sup>^</sup> Scientific Aviation, Boulder, CO, USA  
57 <sup>\*</sup> Institute of Atmospheric Physics, German Aerospace Center, Wessling, Germany  
58 <sup>#</sup> Johannes Gutenberg University, Mainz, Germany  
59 <sup>+</sup> Cooperative Institute for Research in Environmental Sciences, University of Colorado Boulder, Boulder, CO,  
60 USA and NOAA Chemical Sciences Laboratory (CSL), Boulder, CO, USA  
61 <sup>◇</sup> Earth Observing Laboratory, NCAR, Boulder, CO, USA  
62 <sup>x</sup> McKelvey School of Engineering, Washington University, MO, USA

63 *Correspondence to:* ([g.gkatzelis@juelich.de](mailto:g.gkatzelis@juelich.de) and [matthew.m.coggon@noaa.gov](mailto:matthew.m.coggon@noaa.gov))

64 **Abstract.**

65 Extensive airborne measurements of non-methane organic gases (NMOGs), methane, nitrogen oxides, reduced  
66 nitrogen-species, and aerosol emissions from US wild and prescribed fires were conducted during the 2019  
67 NOAA/NASA Fire Influence on Regional to Global Environments and Air Quality campaign (FIREX-AQ). Here,  
68 we report the atmospheric enhancement ratios (ERs) and inferred emission factors (EFs) for compounds measured  
69 onboard the NASA DC-8 research aircraft for nine wildfires and one prescribed fire, which encompass a range of  
70 vegetation types.

71 We use photochemical proxies to identify young smoke and reduce the effects of chemical degradation on our  
72 emissions calculations. ERs and EFs calculated from FIREX-AQ observations agree within a factor of 2 with values  
73 reported from previous laboratory and field studies for more than 80% of the carbon- and nitrogen-containing  
74 species. Wildfire emissions are parameterized based on correlations of the sum of NMOGs with reactive nitrogen  
75 oxides (NO<sub>y</sub>) to modified combustion efficiency (MCE) as well as other chemical signatures indicative of  
76 flaming/smoldering combustion, including carbon monoxide (CO), nitrogen dioxide (NO<sub>2</sub>), and black carbon  
77 aerosol. The sum of primary NMOG EFs correlates to MCE with an R<sup>2</sup> of 0.68 and a slope of  $-296 \pm 51 \text{ g kg}^{-1}$ ,  
78 consistent with previous studies. The sum of the NMOG mixing ratios correlates well with CO with an R<sup>2</sup> of 0.98  
79 and a slope of  $137 \pm 4 \text{ ppbv}$  of NMOGs per ppmv of CO, demonstrating that primary NMOG emissions can be  
80 estimated from CO. Individual nitrogen-containing species correlate better with NO<sub>2</sub>, NO<sub>y</sub>, and black carbon than  
81 with CO. More than half of the NO<sub>y</sub> in fresh plumes is NO<sub>2</sub> with an R<sup>2</sup> of 0.95 and a ratio of NO<sub>2</sub> to NO<sub>y</sub> of  $0.55 \pm$   
82  $0.05 \text{ ppbv ppbv}^{-1}$ , highlighting that fast photochemistry had already occurred in the sampled fire plumes. The ratio  
83 of NO<sub>y</sub> to the sum of NMOGs follows trends observed in laboratory experiments and increases exponentially with  
84 MCE, due to increased emission of key nitrogen species and reduced emission of NMOGs at higher MCE during  
85 flaming combustion. These parameterizations will provide more accurate boundary conditions for modeling and  
86 satellite studies of fire plume chemistry and evolution to predict the downwind formation of secondary pollutants,  
87 including ozone and secondary organic aerosol.

Open biomass burning in the form of wildfires, prescribed forest management fires, and agricultural burns is one of the largest sources of trace gases and aerosols worldwide (Akagi et al., 2011; Crutzen and Andreae, 1990). It is the dominant global source of black carbon and primary organic aerosol (Bond et al., 2013), and accounts for more than 20% of the global emissions of nitric oxide (NO) and carbon monoxide (CO) (Olivier et al., 2005; Yokelson et al., 2008; Wiedinmyer et al., 2011). It is the second largest global source of non-methane organic gases (NMOGs) (Akagi et al., 2011), and a major source of greenhouse gases, including methane (CH<sub>4</sub>), carbon dioxide (CO<sub>2</sub>), and nitrous oxide (N<sub>2</sub>O) that impact the atmospheric carbon budget and climate (Sudo and Akimoto, 2007; Ward et al., 2012; Tian et al., 2016; Le Quéré et al., 2018).

During the last decade, the number of wildfires and prescribed fires in the US has sometimes exceeded 74,000 and 450,000 yr<sup>-1</sup>, respectively (National Interagency Fire Center). Warming temperatures, drier climate, and a history of fire suppression are projected to increase the frequency and intensity of wildfires and lengthen fire seasons globally (Spracklen et al., 2009; Kloster et al., 2010; Pechony and Shindell, 2010; Moritz et al., 2012; Flannigan et al., 2013; Mann et al., 2016; Balch et al., 2017), which is already evident in the western US, Canada, the eastern Mediterranean, Siberia, and Australia (Westerling et al., 2006; Keywood et al., 2013; Yue et al., 2015). Wildfires in the US largely occur in the western conterminous states and Alaska, and typically account for 12 to 40 thousand km<sup>2</sup> of the annual total area burned (National Interagency Fire Center). In the southeastern US, prescribed fires and agricultural burns are a common land management tool used to improve ecosystem health or facilitate planting crops (Wiedinmyer and Hurteau, 2010; Cochrane et al., 2012). Since prescribed fires in the southeast currently account for about 25 thousand km<sup>2</sup> per year on average (National Interagency Fire Center), it is also important to characterize their emissions.

While wildfires and prescribed fires are favorable for many ecosystem functions, the atmospheric impacts of fire on climate, air quality, and health are a major concern. Particles directly emitted or formed via chemical processes have direct and indirect effects on climate by influencing the regional and global radiation balance and impacting cloud properties and precipitation (Braga et al., 2017; Cecchini et al., 2017; Hamilton et al., 2018; Thornhill et al., 2018; Kodros et al., 2020). Global mortality from outdoor pollution due to biomass burning smoke accounts for 600,000 premature deaths per year (Johnston et al., 2012), with particulate matter (PM) and O<sub>3</sub> posing the greatest risk factors (Akagi et al., 2014; Dennekamp et al., 2015; Brey and Fischer, 2015; Knorr et al., 2017; Apte et al., 2018). In smoke plumes, O<sub>3</sub> and secondary organic aerosols are photochemically produced from the interplay of NO<sub>x</sub>, NMOGs, and meteorology (Tsimpidi et al., 2017; Hodshire et al., 2019). An essential first step to elucidate the factors contributing to PM and O<sub>3</sub> pollution downwind fires is to quantify primary gas- and particle-phase emissions.

Numerous studies have quantified emission factors (EFs; grams emitted per kg of dry fuel burned) for various fuel types and different fire characteristics using ground-based or airborne measurements in close proximity to wildland/prescribed fire plumes (e.g., Stockwell et al., 2016; Liu et al., 2017; Peng et al., 2020; Mouat et al., 2022; Lindaas et al., 2021; Permar et al., 2021) or controlled laboratory burns (e.g., Stockwell et al., 2014; Koss et al., 2018; Selimovic et al., 2018). Literature reviews to combine these results have been periodically conducted (Andreae and Merlet, 2001; Akagi et al., 2011; Andreae, 2019), with the most recent by Prichard et al. (2020). Nevertheless, uncertainties in the process-level understanding and model representation of fire emissions, plume rise, and chemistry still exist, which influence model performance in accurately capturing downwind O<sub>3</sub> and secondary organic aerosol formation (Müller et al., 2016; Reddington et al., 2016; Shrivastava et al., 2017). These uncertainties can result from an insufficient understanding of the chemistry and total emissions of NO<sub>x</sub> and NMOGs across fuel types, ecosystems, and fire combustion conditions (Warneke et al., 2011; Yokelson et al., 2013; Hatch et al., 2017).

In this study, we calculate western US wildfire emission factors for a broad range of gas- and particle-phase species measured aboard the NASA DC-8 during the 2019 Fire Influence on Regional to Global Environments and Air Quality (FIREX-AQ) campaign, which included the most comprehensive payload to date for airborne sampling of biomass burning emissions. We compare our results to the most recent laboratory and airborne field studies, including the fire sciences laboratory component of FIREX-AQ (hereafter referred to as FireLab) (Koss et al., 2018), the fourth Fire Lab at Missoula Experiment, FLAME-4 (Stockwell et al., 2015), the Western Wildfire Experiment for Cloud Chemistry, Aerosol Absorption, and Nitrogen, WE-CAN (Permar et al., 2021), and the Studies of

137 Emissions and Atmospheric Composition, Clouds and Climate Coupling by Regional Surveys, SEAC<sup>4</sup>RS (Liu et  
138 al., 2017; Wolfe et al., 2022), as well as results summarised in the review by Andreae (2019). We parameterize  
139 wildfire emissions based on correlations of carbon- and nitrogen-containing species to CO, NO<sub>2</sub>, black carbon, and  
140 modified combustion efficiency (MCE) to improve future modeling efforts to accurately capture the chemical  
141 evolution of wildfire smoke.

## 142 2 Methods

### 143 2.1 Platforms and Instrumentation

144 The NASA DC-8 aircraft was deployed with an extensive suite of instruments to measure the gas- and particle-  
145 phase pollutants emitted and photochemically produced downwind of US wildfires. Figure 1 and Table 1 show the  
146 research flights analyzed here to capture freshly emitted wildfire smoke from 22 July to 3 September 2019. In total,  
147 16 crosswind plume transects downwind from 9 western wildfires and 1 eastern prescribed fire are analyzed, which  
148 represent a range of fuel types, including timber, grass, dead trees, logging debris, brush, and litter. The transects  
149 are selected based on aging proxies to examine emissions with minimal atmospheric processing. The physical age  
150 is determined based on transect proximity to the fire, an estimated plume rise time, and wind speed (Holmes et al.,  
151 2020) and ranged from 10–153 min (1–40 km) downwind for the plumes described here. The MCE, defined as  
152  $\Delta\text{CO}_2/(\Delta\text{CO}_2+\Delta\text{CO})$ , is commonly reported to quantify the fire conditions and describes the relative amount of  
153 flaming and smoldering combustion (Yokelson et al., 1996). Pure flaming fires have an MCE near 0.99, while  
154 smoldering fires vary over a wider range but are most often near 0.8 (Akagi et al., 2011). For the freshest plume  
155 crossings, the MCE was on average  $0.90 \pm 0.04$  (range 0.94–0.85), suggesting a mix of flaming and smoldering  
156 emissions.



157  
158 **Figure 1:** Selected NASA DC-8 flight tracks for sampling the wildfire and prescribed fire plumes during the 2019 FIREX-AQ.  
159 Fires discussed in this study are denoted by black markers. The US map is colored by land cover classification.

160 Multiple instruments performed measurements of gas- and particle-phase species summarized in Table 2. The  
161 University of Colorado aircraft aerosol mass spectrometer (CU HRAMS, AMS in the following) (Canagaratna et  
162 al., 2007; Guo et al., 2021) measured organic aerosol, particulate ammonium, and nitrate (pNO<sub>y</sub>) that consisted of  
163 inorganic nitrates (pNO<sub>3</sub>), organic nitrates (pRONO<sub>2</sub>), and nitroaromatics (pArNO<sub>2</sub>) (Day et al., 2022). Black carbon  
164 aerosol concentration was measured by a Single-Particle Soot Photometer (SP2) and scaled (~10%) to represent the  
165 total accumulation-mode (Schwarz et al., 2008). NMOGs were measured by the NOAA proton transfer reaction  
166 time-of-flight mass spectrometer (PTR-ToF-MS) (Yuan et al., 2016), two whole-air samplers, namely the NOAA  
167 integrated Whole Air Sampler (NOAA iWAS; <10 second sample time) (Lerner et al., 2017) and the University of

168  
169

California, Irvine Whole Air Sampler (UCI WAS; < 40 second sample time) (Colman et al., 2001; Simpson et al., 2020), the NCAR Trace

170  
171  
172

**Table 1:** Freshest plume crossings identified for analysis during FIREX-AQ 2019. Forest and shrubland fuel types were determined using the FCCS database, while cropland fires were classified with the Cropland Data Layer and DC-8 overflight videos (Warneke et al., 2022).

| Fire                          | Transect number | Date and Time, UTC | Fuel Type   | Maleic anhydride to furan as an indicator of OH exposure (ppb ppb <sup>-1</sup> ) | Physical age (s) | MCE  |
|-------------------------------|-----------------|--------------------|---|---|------------------|------|
| Shady                         | 0               | 7/25/2019 22:48    | Understory: Ponderosa pine, white-Douglas fir, quaking aspen, two-needle pinyon-Utah juniper forest w/ open shrubs, grasses, and timber litter          | 0.09  | 1350             | 0.91 |
| Shady                         | 9               | 7/25/2019 23:47    |   | 0.07  | 1250             | 0.90 |
| North Hills                   | 0               | 7/29/2019 23:21    | Savanna: Ponderosa pine savanna, Douglas-fir-Pacific ponderosa pine, ocean spray forest with Idaho fescue-bluebunch wheatgrass                          | 0.13  | 600              | 0.86 |
| Tucker                        | 0               | 7/30/2019 2:40     | Shrubland: Sagebrush-greasewood shrubland with open grasses   | 0.12  | 1720             | 0.91 |
| Ridgetop                      | 4               | 8/2/2019 23:18     | Grassland: Bluebunch wheatgrass, bluegrass with sagebrush-greasewood shrubs and savanna   | 0.14  | 2620             | 0.94 |
| Lick Creek                    | 1               | 8/3/2019 1:13      | Forest: Grand-Douglas fir, Pacific ponderosa pine, ocean spray forest   | 0.15  | 1500             | 0.91 |
| Williams Flats                | 0               | 8/3/2019 22:22     | Grassland: Idaho fescue-bluebunch wheatgrass-cheatgrass, sagebrush shrublands under open Douglas-fir-Pacific ponderosa pine, ocean spray savanna/forest | 0.16  | 890              | 0.91 |
| Williams Flats                | 21              | 8/4/2019 0:41      |   | 0.14  | 6130             | 0.91 |
| Horsefly                      | 1               | 8/6/2019 23:20     | Forest: Managed: Subalpine-Douglas fir, lodgepole-whitebark-Pacific ponderosa-Mature lodgepole pine, Engelmann spruce oceanspray forest                 | 0.12  | 3890             | 0.87 |
| Horsefly                      | 3               | 8/6/2019 23:28     |   | 0.11  | 6250             | 0.85 |
| Williams Flats                | 7               | 8/9/2019 1:49      | Forest: Douglas-fir-Pacific ponderosa pine, ocean spray forest with grassland understory  | 0.11  | 5460             | 0.91 |
| Castle                        | 0               | 8/13/2019 0:18     | Forest: Ponderosa pine, two-needle-pinyon-Utah juniper, Douglas-white fir, Madrean pine-oak, quaking aspen forest                                       | 0.15  | 1540             | 0.90 |
| Castle                        | 0               | 8/13/2019 23:17    |   | 0.16  | 9200             | 0.90 |
| Castle                        | 10              | 8/14/2019 1:32     |   | 0.07  | 1600             | 0.88 |
| Sheridan                      | 1               | 8/17/2019 0:42     | Forest: Pinyon-Utah juniper forest with Turbinella oak-alderleaf mountain mahogany shrubland  | 0.15  | 1200             | 0.91 |
| Blackwater River State Forest | 8               | 8/30/2019 17:11    | Forest: Prescription, primarily shrubs, grasses and litter from loblolly-longleaf-slash pine, willow-laurel-turkey-water oak, and magnolia forest       | 0.31  | 580              | 0.93 |

173

**Table 2:** Descriptions of the instrumentation aboard the NASA DC-8 used in this study.

| Species Measured                                       | Technique         | Frequency [Hz] | Inlet Setup  | Reference             |
|--|-------------------|----------------|--|-----------------------|
| O <sub>3</sub> , NO, NO <sub>2</sub> , NO <sub>y</sub> | Chemiluminescence | 1              | PFA, approx. 1 m long, 1 slpm for each species; NO and NO <sub>2</sub> additionally pass through 50.9 cm <sup>3</sup> quartz cells | Ryerson et al. (2000) |

|  |  |                                     |  |   |
|--|--|-------------------------------------|--|---|
| CO <sub>2</sub> , CO, CH <sub>4</sub> , H <sub>2</sub> O   | 2x Laser Absorption Spectroscopy             | 1-5                                 | ¼ in stainless steel, 2 m long, 3slpm flow   | <i>Sachse et al. (1991)</i><br><i>Bourgeois et al. (2022)</i> |
| NH <sub>3</sub> , speciated hydrocarbons and OVOCs   | PTR-ToF-MS                                   | 1 (NH <sub>3</sub> )<br>10 (others) | PFA, 2 m long, ~20 LPM (before Aug 3), ~60 LPM (from Aug 3 onwards), heated to 60°C  | <i>Müller et al. (2016)</i><br><i>(with modifications)</i>    |
| PAN, PPN, other PANs   | Chemical Ionization Mass Spectrometry (CIMS) | 1-10                                | ½" FEP tubing  | <i>Zheng et al. (2011)</i>                                    |
| HONO, HCN, HNCO, HCOOH, N <sub>2</sub> O <sub>5</sub> , HPMTF, halogenated compounds   | Iodide ToF-CIMS                              | 1                                   | PTFE, 1m long, 6 SLPM, heated to 40°C  | <i>Veres et al. (2020)</i>                                    |
| NO   | Laser Induced Fluorescence                   | 1                                   | PFA and silcosteel, 1m length, unheated, overflow at 10-20 slm   | <i>Rollins et al. (2020)</i>                                  |
| CH <sub>2</sub> O, C <sub>2</sub> H <sub>6</sub>   | Laser Absorption Spectroscopy                | 1                                   | Heated HIAPER Inlet followed by several meters of heated PTFE Teflon tubing  | <i>Richter et al. (2015);</i><br><i>Fried et al. (2020)</i>   |
| C <sub>2</sub> -C <sub>10</sub> Alkanes, C <sub>2</sub> -C <sub>4</sub> Alkenes, C <sub>6</sub> -C <sub>9</sub> Aromatics, C <sub>1</sub> -C <sub>5</sub> Alkyl nitrates, etc. | Whole Air Sampling                           | Up to 168 per flight                | stainless steel  | <i>Simpson et al. (2001)</i>                                  |
| Speciated hydrocarbons and OVOCs   | H <sub>3</sub> O <sup>+</sup> ToF-CIMS       | 1-5                                 | PTFE, 1m long, 1-2 LPM, heated to 50°C   | <i>Yuan et al. (2016)</i>                                     |
| C <sub>2</sub> -C <sub>10</sub> Alkanes, C <sub>2</sub> -C <sub>4</sub> Alkenes, C <sub>6</sub> -C <sub>9</sub> Aromatics, C <sub>1</sub> -C <sub>5</sub> Alkyl nitrates, etc. | Whole Air Sampling                           | Up to 72 per flight                 | PFA, 2m Long, ~60 LPM, unheated  | <i>Lerner et al. (2017)</i>                                   |
| C <sub>3</sub> -C <sub>10</sub> hydrocarbons, C <sub>1</sub> -C <sub>7</sub> OVOCs, HCN, CH <sub>3</sub> CN, halogenated VOCs, etc.  | HR-ToF-GC/MS                                 | 0.0095                              | Restek Silcosteel, 2.5 LPM, heated to 40°C   | <i>Apel et al. (2010)</i>                                     |
| CH <sub>2</sub> O  | Laser Induced Fluorescence                   | 1-10                                | PFA and silcosteel, 1m length, unheated, overflow at 10-20 slm   | <i>Cazorla et al. (2015)</i>                                  |
| H <sub>2</sub> O <sub>2</sub> , organic peroxides, organic acids, isoprene oxidation products, etc.  | CIMS   | 1                                   | A glass tube (3 cm ID and 47cm long) coated with a thin layer of (Fluoropel PFC 801A, Cytonix Corp.). The tube is gently heated and the sampling flow rate through the glass tube is >=40 m/s. | <i>Crouse et al. (2006)</i>                                   |
| glyoxal, methylglyoxal, HONO, NO <sub>2</sub>  | Airborne Cavity Enhanced Spectrometer        | 1                                   | PTFE Teflon, <1 m length, inlet heated to 25°C, 10.5 vlpn  | <i>Min et al. (2016)</i>                                      |
| BC mass concentration  | SP2  | 1                                   | NASA Langley inlet with optional dilution  | <i>Schwarz et al. (2008)</i>                                  |
| Submicron aerosol composition  | CU-HR-AMS                                    | 1 (up to 10 Hz in plumes)           | HIMIL tall inlet, 1.3 m SS 0.18" ID+ 0.45 m 0.08" ID tubing + pressure controlled instrument inlet (<0.3 s total residence time)   | <i>Guo et al (2021);</i><br><i>Canagaratna et al (2007)</i>   |

174 Organic Gas Analyzer (Apel et al., 2015), a fast online gas chromatograph outfitted with a Time-of-Flight mass  
175 spectrometer (TOGA-TOF; < 35 second sample time), the Caltech chemical ionization time-of-flight mass  
176 spectrometer (CIT-ToF-CIMS), and for selected flights the University of Innsbruck / University of Oslo  
177 (UIBK/UiO) PTR-ToF-MS (prototype PTR-TOF 4000X2; IONICON Analytik GmbH, Innsbruck, Austria). Three  
178 instruments were used in this study that measured formaldehyde: the In Situ Airborne Formaldehyde (ISAF)  
179 instrument (Liao et al., 2021), the Compact Atmospheric Multispecies Spectrometer (CAMS) (Weibring et al.,  
180 2007), and the UIBK/UiO PTR-ToF-MS. ISAF and CAMS correlated with an R<sup>2</sup> coefficient of 0.99 and a slope of

181 1.27, as discussed by Liao et al. (2021); whereas the UIBK/UiO PTR-ToF-MS agreed better with the CAMS, with  
182 a slope of 1.02. In this study, we use the ISAF measurements, which have the best time response compared to all  
183 other instruments and adjust the mixing ratios to match those reported by CAMS and the UIBK/UiO PTR-ToF-MS.  
184 The NOAA Iodide ion chemical ionization mass spectrometer (NOAA CIMS) (Veres et al., 2020; Robinson et al.,  
185 2022) was used to measure formic acid (HCOOH), nitrous acid (HONO), and dinitrogen pentoxide (N<sub>2</sub>O<sub>5</sub>). CO and  
186 CH<sub>4</sub> were measured via mid-IR wavelength modulation spectroscopy by the Differential Absorption Carbon  
187 Monoxide Measurement (DACOM) instrument (Sachse et al., 1991). CO<sub>2</sub> was measured via nondispersive infrared  
188 absorption spectroscopy using a LICOR model 7000 analyzer (Vay et al., 2009). NO, NO<sub>2</sub>, and NO<sub>y</sub> were measured  
189 by the NOAA chemiluminescence instrument (Bourgeois et al., 2020). NO<sub>y</sub> measures the sum of reactive nitrogen  
190 compounds, including NO, NO<sub>2</sub>, HONO, peroxy nitrates, alkyl and multifunctional nitrates, and particulate nitrate.  
191 Additional measurements of HONO and NO<sub>2</sub> were provided by the NOAA Airborne Cavity Enhanced Spectrometer  
192 (ACES) (Min et al., 2016) and NO by the NOAA Laser Induced Fluorescence instrument (NO-LIF) (Rollins et al.,  
193 2020). Glyoxal and methylglyoxal were measured by ACES, and ammonia (NH<sub>3</sub>) by the UIBK/UiO PTR-ToF-MS  
194 (Müller et al., 2016; Tomsche et al., 2023). The Georgia Tech CIMS (GT-CIMS) was used to measure peroxyacetyl  
195 nitrate (PAN) and other PAN-like compounds such as peroxypropionyl nitrate, peroxyacryloyl nitrate, and  
196 peroxybutyryl nitrate. Finally, the plume structure was obtained from aerosol backscatter measured with the NASA  
197 Langley Airborne Differential Absorption Lidar (DIAL). All measurements reported here are provided in the NASA  
198 FIREX-AQ data repository (NASA airborne science data for atmospheric composition, 2019).

199 In this study, we focus on quantifying total and speciated NMOG emissions, which were predominantly measured  
200 by PTR-ToF-MS, the two Whole Air Samplers, and the Trace Organic Gas Analyzer with Time-of-Flight mass  
201 spectrometer (TOGA-TOF). The same NOAA PTR-ToF-MS and the iWAS systems were used at the US Forest  
202 Service's Missoula Fire Sciences Laboratory (FireLab) in 2016 as a precursor to FIREX-AQ and described by Koss  
203 et al. (2018). Koss et al. (2018) speciated isomers measured by PTR-ToF-MS using gas chromatography pre-  
204 separation and reported isomer distributions for over 150 individual masses. Here, we compare these isomer  
205 distributions to the speciation derived based on the comparison of the GC-MS and PTR-ToF-MS measurements  
206 conducted aboard the NASA DC-8 (Table S5). Two calibration methods were used to determine NMOG sensitivities  
207 for the PTR-ToF-MS. For commercially available compounds, sensitivities were determined by gravimetrically  
208 prepared standards or by liquid calibration, as described by Coggon et al. (2019). Sensitivities for other species were  
209 estimated based on calculated proton transfer rate coefficients, as described by Sekimoto et al. (2017). For the WAS  
210 system(s), NMOGs were calibrated using gravimetrically prepared standards, as described by Lerner et al. (2017).  
211 A detailed description of the PTR-ToF-MS and WAS setups as well as NMOG uncertainty is included in the  
212 supplement.

## 213 **3 Results and discussion**

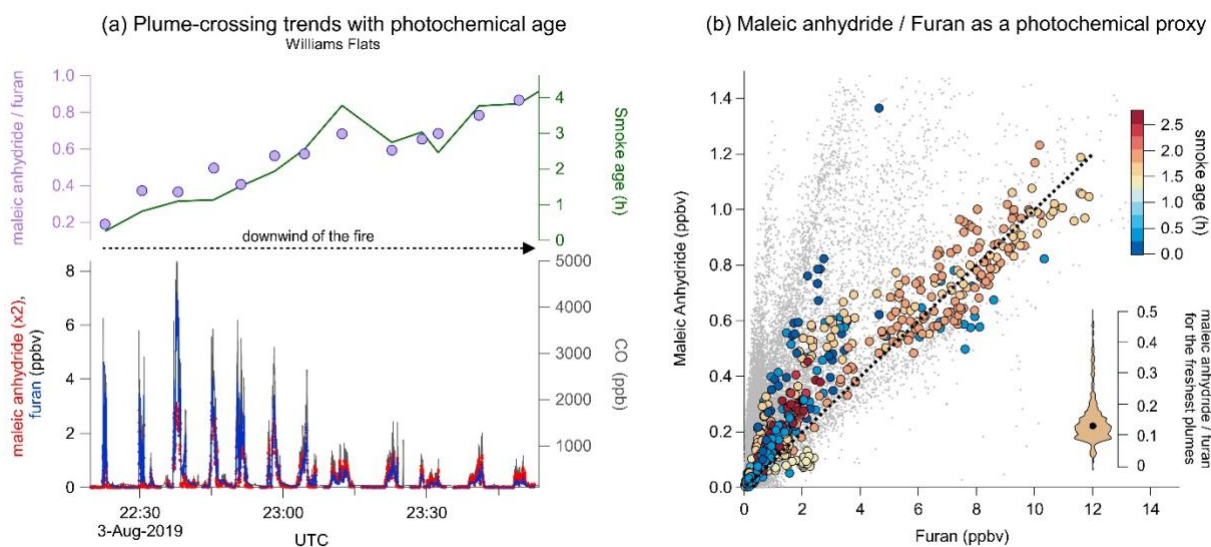
### 214 **3.1 Plumes with minimal photochemical aging**

215 Emissions from wildfire plumes chemically transform once injected into the atmosphere (e.g., Akagi 2012;  
216 Robinson et al., 2021; Decker et al., 2021; Xu et al., 2021). However, safety and operational constraints limit the  
217 proximity of airborne sampling to the fire. An essential first step to quantifying wildfire primary emissions is to  
218 identify plume samples that have undergone minimal chemical processing. Commonly, the freshest plumes are  
219 identified using the plume age calculated from the distance downwind of the wildfire using the onboard measured  
220 average wind speed (e.g., Permar et al., 2021) but neglecting plume rise. The physical age does not necessarily  
221 identify plume crossings with the least chemical processing since the sampled smoke can be impacted by  
222 meteorology, solar radiation, radical concentrations, and sampling artifacts related to the aircraft's position relative  
223 to the center of the plume (Robinson et al., 2021; Decker et al., 2021; Wang et al., 2021).

224 Here, we account for oxidation by hydroxyl radical (OH) using the ratio of primary and secondary NMOG wildfire  
225 tracers, specifically furan (a primary species; Koss et al., 2018) and maleic anhydride (a slow-reacting, secondary  
226 species observed downwind of fires) (Zhao and Wang, 2017). Coggon et al. (2019) show that maleic anhydride  
227 quickly forms downwind of fires from the OH oxidation of furans, and Wang et al. (2021) show that the distribution  
228 of maleic anhydride in plumes closely mirrors the distribution of OH exposure. Since furan is a direct wildfire  
229 emission and maleic anhydride is a chemical product of furan chemistry that is not significantly emitted from fires

230 (Coggon et al., 2019; Wang et al., 2021), the ratio of maleic anhydride to furan (MA/F) is expected to increase  
 231 downwind of a fire and exhibit a minimum in the least-processed plumes. This ratio is used as a photochemical  
 232 proxy to identify the freshest sampled plumes by extracting the lowest MA/F transect per wildfire plume and reduce  
 233 the effects of chemical degradation on our primary NMOG emission calculations. We note that this technique may  
 234 not account for the faster photolysis of light-absorbing species (such as HONO) or fast interconversion between NO  
 235 and NO<sub>2</sub>, though the sum of reactive nitrogen species (NO<sub>x</sub>) is expected to be conserved downwind of fires (Lindaas  
 236 et al., 2020). We note that a quantitative relationship between MA/F and OH exposure is not presented here as the  
 237 yield of maleic anhydride from furan oxidation requires further laboratory quantification. Other furans also produce  
 238 maleic anhydride (Coggon et al., 2019), and thus the MA/F ratios used here is simply a proxy for screening out  
 239 significantly processed emissions.

240 Figure 2a shows the maleic anhydride, furan, and CO concentration downwind of the Williams Flats wildfire on 3  
 241 August 2019, as a characteristic example. Figure 2b shows the relationship between maleic anhydride and furan for  
 242 all of the plume-crossings sampled during FIREX-AQ. The freshest crossings for each fire are highlighted as circles  
 243 colored by the estimated smoke age. Also shown are the MA/F and the median physical smoke age calculated for  
 244 each plume crossing. Here we use the high time resolution of PTR-ToF-MS for MA and furan concentrations, but  
 245 furan is additionally scaled by 0.46 to match the TOGA GC-MS concentrations as discussed in Sect. 3.2. VOC and  
 246 CO concentrations were highest closer to the wildfire and decreased downwind, primarily due to dilution. During  
 247 the Williams Flats (Fig. 2a), the MA/F increased from 0.20 to 0.86 downwind of the fire, indicating active chemical  
 248 conversion of furan to maleic anhydride. The physical smoke age followed the same increase from 0.5 to 4 hours.  
 249 Figure 2b shows that the MA/F for all of the freshest plume crossings had a median of 0.13 (0.10–0.16, 25th–75th),  
 250 and their corresponding physical age was less than 1.46 h (0.6–1.74) (see Table 1). It is notable that certain fires  
 251 with similar MA/F ratios ranged in physical age from 15 minutes to as high as 3–4 hours. These differences show  
 252 how chemical processing in some plumes may be slow over long-distances, while other plumes may undergo  
 253 immediate oxidation. Despite these differences, the majority of chemically fresh plumes sampled during FIREX-  
 254 AQ exhibited very similar MA/F ratios (Fig. 2b).



255  
 256 **Figure 2:** (a) Mixing ratios of maleic anhydride, furan, and CO (bottom) and ratios of maleic anhydride to furan (top) in 12  
 257 crosswind plume transects of smoke from the Williams Flats fire on 3 August 2019. The maleic anhydride to furan ratio increases  
 258 as the plume ages during transport away from the Williams Flats. (b) Comparison of the maleic anhydride and furan mixing  
 259 ratios used as a photochemical proxy to identify the freshest plume crossings during FIREX-AQ. Grey points are all 1-second  
 260 resolution measurements during FIREX-AQ, and circles are the chosen freshest plume crossings colored by the physical smoke  
 261 age. The violin plot shows the variability of the ratio of maleic anhydride to furan for the freshest wildfire transects.

262 Figure S1 further highlights differences in the physical and chemical age of a fire by focusing on the Williams Flats  
 263 wildfire and the Blackwater prescribed fire. The DIAL image shows the shape and evolution of the wildfire smoke  
 264 from overpass flights. For the Williams Flats fire, the DC-8 sampled emissions by performing raster patterns



265 perpendicular to the smoke, whereas for the Blackwater fire, the DC-8 also flew along the smoke plume at various  
266 altitudes. For the Blackwater fire, the MA/F increased rapidly up to 1.4 ppbv ppbv<sup>-1</sup> 30 km downwind of the wildfire,  
267 while for the Williams Flats fire, the ratio reached a maximum of 1 ppbv ppbv<sup>-1</sup> 120 km downwind of the fire. These  
268 differences further highlight the importance of accounting for the chemical rather than the physical age of a fire to  
269 determine the freshest transects.

270 The MA/F for fresh, unaged smoke during the FireLab study was ~ 0.04 ppbv ppbv<sup>-1</sup> (Wang et al., 2021), showing  
271 that even the freshest plume transects sampled during FIREX-AQ were photochemically processed to some extent.  
272 For the remainder of this analysis, fire plumes sampled closest to the emission source that exhibited a MA/F > 0.20  
273 are excluded from the calculation of emission ratios and enhancements. This cut-off is based on the median MA/F  
274 ratio observed for the freshest plume plumes sampled during FIREX-AQ (0.13 ppbv ppbv<sup>-1</sup>, Fig. 2b). The exception  
275 is the Blackwater prescribed fire that was the only fire representative of southeastern US fuel types included in our  
276 analysis, even though the freshest plume crossing had a MA/F of 0.3. Further evaluation of biases during FIREX-  
277 AQ for fast-reacting species is discussed in Sect. 3.3.

### 278 3.2 Instrument comparisons

279 NMOG measurements obtained from the NOAA PTR-ToF-MS were compared to other instruments onboard the  
280 DC-8, including TOGA-TOF, 2 WAS systems, CIT-CIMS, UIBK/UiO PTR-ToF-MS, and NOAA CIMS. Table S5  
281 provides correlations of the PTR-ToF-MS measurements to other instruments. For calibrated compounds, the  
282 NOAA PTR-ToF-MS and the UIBK/UiO PTR-ToF-MS agreed within 10–35% for methanol, acetonitrile, acetone,  
283 methyl ethyl ketone (MEK), benzene, toluene, C<sub>8</sub> and C<sub>9</sub> aromatics, and monoterpenes. The NOAA PTR-ToF-MS,  
284 and NOAA CIMS agreed within uncertainty for hydrogen cyanide (HCN), isocyanic acid (HNCO), and formic acid,  
285 respectively. CIT-CIMS agreed with the NOAA PTR-ToF-MS for HCN whereas for phenol it was lower by a factor  
286 2. Both instruments were calibrated for phenol suggesting that differences could be due to PTR-ToF-MS  
287 fragmentation of higher molecular weight gases that produce signals at the phenol ion mass, or differences in the  
288 detection of other isomers from the two instruments.

289 Although the PTR-ToF-MS provides high time resolution measurements, it cannot speciate NMOG isomers detected  
290 at the same exact mass. In the following, we compare mixing ratios derived for the PTR-ToF-MS chemical formula  
291 to the combined isomer signals derived from GC-MS, given in parentheses. When compared to the iWAS, WAS,  
292 and TOGA-TOF measurements, the NOAA PTR-ToF-MS was within ±25–35% for CH<sub>4</sub>O (methanol), C<sub>2</sub>H<sub>3</sub>N  
293 (acetonitrile), C<sub>2</sub>H<sub>4</sub>O (acetaldehyde), C<sub>2</sub>H<sub>6</sub>O (ethanol), C<sub>6</sub>H<sub>6</sub> (benzene), C<sub>7</sub>H<sub>8</sub> (toluene), C<sub>3</sub>H<sub>3</sub>N (acrylonitrile),  
294 C<sub>3</sub>H<sub>4</sub>O (acrolein), C<sub>3</sub>H<sub>6</sub>O (acetone + propanal), C<sub>8</sub>H<sub>10</sub> (ethylbenzene + m-, p-, and o-xylenes), and C<sub>4</sub>H<sub>6</sub>O (methyl  
295 vinyl ketone + methacrolein + 2-butenal). However, the NOAA PTR-ToF-MS was higher by a factor of 2 or more  
296 for C<sub>2</sub>H<sub>6</sub>S (dimethyl sulfide), C<sub>4</sub>H<sub>5</sub>N (pyrrole + butene nitrile isomers), C<sub>4</sub>H<sub>4</sub>O (furan), C<sub>3</sub>H<sub>6</sub>O<sub>2</sub> (methyl acetate +  
297 ethyl formate + hydroxyacetone), C<sub>5</sub>H<sub>6</sub>O (2-methyl-furan + 3-methyl-furan), C<sub>5</sub>H<sub>4</sub>O<sub>2</sub> (furfural + 3-furaldehyde),  
298 and C<sub>10</sub>H<sub>16</sub> (monoterpenes) whereas CH<sub>3</sub>NO<sub>2</sub> (nitromethane) agreed with the WAS but was lower than TOGA-TOF.

299 The discrepancies between the GC-MS techniques and PTR-ToF-MS for a number of key species, such as furans,  
300 generally show that the PTR-ToF-MS measures more signal than what can be accounted for by GC-MS. This  
301 observation likely results from a combination of (a) PTR-ToF-MS fragmentation of higher molecular weight gases  
302 that produce signals at parent ion masses, (b) the detection of isomers that cannot elute through a GC column, and  
303 (c) the detection of molecules that are lost to canister sampling. To investigate the causes of these discrepancies,  
304 Table S5 shows isomer distributions for masses detected by the PTR-ToF-MS that are known to represent the sum  
305 of two or more overlapping isomers. These isomer distributions are calculated from the ratio of GC-MS  
306 measurements to the corresponding PTR-ToF-MS mass. Each ratio represents the fraction of the total signal  
307 measured by PTR-ToF-MS that is associated with a given isomer. For example, GC-MS measurements identify 2-  
308 methylfuran and 3-methylfuran as the key isomers with the molecular formula C<sub>5</sub>H<sub>6</sub>O. The slope of isomers to PTR-  
309 ToF-MS measurements of C<sub>5</sub>H<sub>6</sub>O represents the isomer fraction detected by PTR-ToF-MS.

310 The isomer distributions shown in Table S5 are compared to those reported for laboratory smoke by Koss et  
311 al. (2018). Koss et al. (2018) assigned PTR-ToF-MS masses based on literature searches, intercomparisons of PTR-  
312 ToF-MS measurements to other in situ instrumentation, and offline analysis by coupling GC effluent of sampled

313 smoke to the inlet of the PTR-ToF-MS (combined instrumental setup termed GC-PTR-ToF-MS). For low molecular  
314 weight gases known to elute through a GC column, Koss et al. (2018) assigned isomer distributions based on the  
315 total signal detected by GC-PTR-ToF-MS, which includes signals from parent ions produced from proton-transfer  
316 as well as fragments from higher molecular weight gases that elute through a GC. For example, at  $C_5H_6O-H^+$  ( $m/z$   
317 83.0491), 51% of the signal resulted from the elution of 2-methylfuran, 9% resulted from 3-methylfuran, and 37%  
318 was associated with other peaks in the chromatogram that produced signals at  $C_5H_6O-H^+$  (unidentified isomers +  
319 fragments of higher masses). We note that the PTR-ToF-MS instrument employed in this study is the same as that  
320 used by Koss et al. (2018) and is operated with the same drift field ( $E/N = 120$  Td).

321 For species measured during FIREX-AQ where the PTR-ToF-MS reported significantly more mass than the GC  
322 instruments, we find that the isomer distributions derived in this study significantly differ from those derived by  
323 Koss et al (2018) (Table S5). This is most pronounced for the monoterpenes but also the furanoic species, such as  
324 furan ( $C_4H_4O$ ), methylfurans ( $C_5H_6O$ ), and furfurals ( $C_5H_4O_2$ ). Hatch et al. (2017) showed that more than 30  
325 different isomers can contribute to the monoterpenes signal based on two dimensional GC. However, the  
326 conventional GC instruments used during FIREX-AQ could only detect a fraction of these isomers. Furthermore,  
327 differences in sensitivity for the different isomers would further increase the quantification uncertainties for both  
328 GC and PTR-ToF-MS. For the furanoic masses, the PTR-ToF-MS measures a higher fraction of unknown isomers  
329 and fragments than what is reported by Koss et al. (2018). This result holds whether comparing against isomer  
330 distributions derived using TOGA (an online GC method) or WAS methods (a canister sampling method),  
331 suggesting that uncertainties due to differences in calibration are small. These results suggest that the total signal of  
332 furans measured by PTR-ToF-MS during FIREX-AQ is likely influenced by gases that cannot pass through a GC  
333 column, which includes the possibility of unidentified isomers and fragments from higher molecular weight species.  
334 We note that this result is not specific to the PTR-ToF-MS used in this study, as the agreement between the NOAA  
335 PTR-ToF-MS and UIBK/UiO PTR-ToF-MS for these masses is within 3% (Table S5).

336 Furans are an important contributor to VOC reactivity and significantly contribute to the formation of ozone and  
337 other secondary gases (Gilman et al., 2015; Hatch et al., 2017; Coggon et al., 2018). For models employing emission  
338 factors of furans, we recommend using emission factors derived using GC-based methods given that multiple  
339 isomers can be detected with PTR-TOF-MS at the furan mass. This also applies to other specific compound classes.  
340 In Table S1, we include the methods used in this study to derive emission factors. For applications where the fast  
341 time-resolution from PTR-ToF-MS is needed (e.g., in deriving cross-plume trends in gases), (Decker et al. 2021; Xu  
342 et al. 2021), the interpretation of trends in furans should include the possibility of unknown isomers and fragments.

### 343 **3.3 Emission ratios and emission factors of US wildfire smoke**

344 The freshest plume transects are used to estimate the primary emissions for individual fires. Table 3 shows the  
345 average compound-specific enhancement ratios to CO which we interpret as emission ratios (ERs) for most species,  
346 and the inferred emission factors (EFs) calculated for more than 100 species and groups of species from the freshest  
347 wildfire plume transects sampled during FIREX-AQ. ERs and EFs for each fire are also calculated and provided in  
348 Tables S2 and S3. Given that fast chemistry already occurred in some fire transects, the ER and EF estimates of  
349 highly reactive species like HONO are lower bounds. ERs are the slope of a linear fit of each species with CO  
350 mixing ratios (see Sect. S1). EFs were calculated following Eq. (1):

$$351 \quad EF_i = F_C \cdot \frac{MM_i}{AW_C} \cdot \frac{\Delta i/\Delta CO}{\sum_{x=1}^n (NC_x \cdot \frac{\Delta C_x}{\Delta CO})}, \quad (1)$$

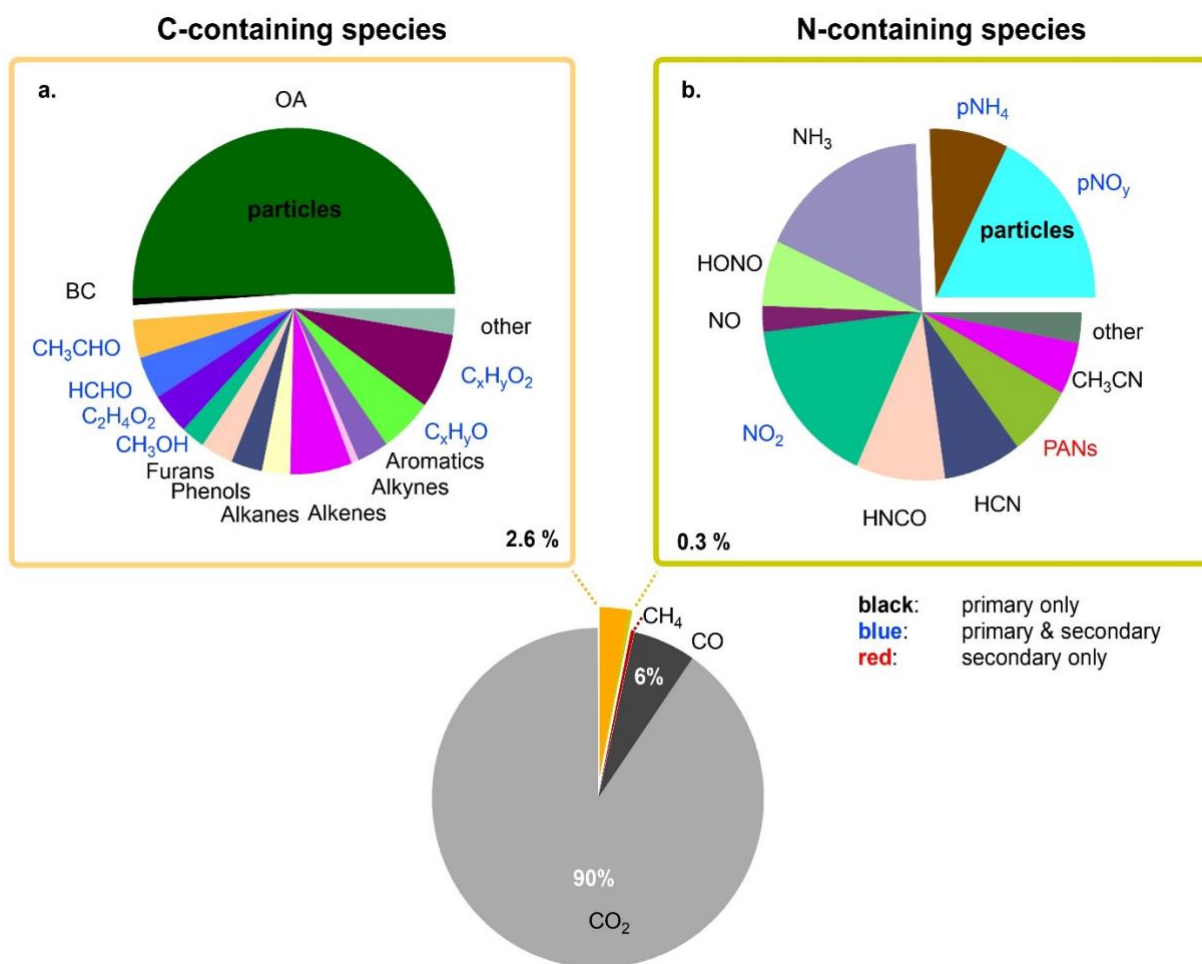
352 where  $EF_i$  is the emission factor of compound  $i$  calculated similarly to Akagi et al. (2011);  $F_C$  is the carbon fraction  
353 of the fuel assumed to be  $0.5 \text{ g g}^{-1}$ ;  $MM_i$  is the molar mass of  $i$ ;  $AW_C$  is the atomic mass of carbon ( $12 \text{ g mol}^{-1}$ );  
354  $\Delta i/\Delta CO$  is the emission ratio of a compound relative to CO;  $NC_x$  is the number of carbon atoms in C-containing  
355 species  $x$ , and  $\Delta C_x/\Delta CO$  is the emission ratio of species  $x$  to CO. This method assumes that all the carbon lost from  
356 the fuel as it burns is emitted and measured, which is a reasonable approximation as CO, CO<sub>2</sub>, and CH<sub>4</sub> account for  
357 most of the emitted carbon (Akagi et al., 2011). The denominator of the last term estimates total carbon relative to  
358 CO. Species  $C_x$  includes all species shown in Table 3. The carbon not quantified by the suite of instrumentation

359  
360

available during FIREX-AQ likely results in emission factor overestimates no more than 1–2% (Yokelson et al., 2013; Stockwell et al., 2015).

361  
362  
363  
364  
365  
366  
367  
368  
369  
370  
371  
372  
373  
374  
375  
376  
377  
378

Figure 3 shows the average chemical composition of freshly emitted wildfire smoke in  $\text{g kg}^{-1}$  (see Eq. (1)).  $\text{CO}_2$ ,  $\text{CO}$ , and  $\text{CH}_4$  are 97% of the total mass. The remaining 3% consisted of gas- and particle-phase carbon-containing (C-containing, 2.6%) and nitrogen-containing (N-containing, 0.3%) species. 50.4% and 0.7% of this remaining C-containing total mass results from organic aerosol and black carbon (BC), respectively. In the gas phase, 6.4% of the remaining C-containing species mass, which includes all species in Fig. 3a, were phenolic compounds and furans, 4% formaldehyde (HCHO), 4% glycolaldehyde and acetic acid ( $\text{C}_2\text{H}_4\text{O}_2$ ), 3.7% acetaldehyde ( $\text{CH}_3\text{CHO}$ ), 2.1% methanol, 5.8% remaining compounds with one oxygen atom ( $\text{C}_x\text{H}_y\text{O}$ ), 6.9% remaining compounds with two oxygen atoms ( $\text{C}_x\text{H}_y\text{O}_2$ ), 3.1% aromatics, 6.3% alkenes, 2.8% alkanes, and 3.3% other species. N-containing species mass, shown in Fig. 3b, consisted of organic and inorganic nitrate, and other organic nitro compounds such as nitroaromatics ( $\text{pNO}_y$ , 19%) and ammonium ( $\text{pNH}_4^+$ , 8.5%) in the particle-phase; whereas, the dominant gas-phase N-containing species mass was from ammonia ( $\text{NH}_3$ , 18.5%), followed by nitrogen dioxide ( $\text{NO}_2$ , 17.5%), isocyanic acid ( $\text{HNCO}$ , 8.5%), hydrogen cyanide ( $\text{HCN}$ , 5%), peroxyacyl nitrates (PANs, 7%), nitrous acid ( $\text{HONO}$ , 4.8%), nitric oxide ( $\text{NO}$ , 2.5%), and others at 3%. The high contribution of  $\text{NO}_2$  in comparison to  $\text{NO}$  and  $\text{HONO}$ , and the existence of secondary pollutants, in particular PANs, also indicate that chemistry occurred from the time of emission to the time of detection. Given the fast conversion of  $\text{NO}$  and  $\text{HONO}$  to  $\text{NO}_2$  and nitrate, and  $\text{NH}_3$  to particulate ammonium, we also include in Table 3 the conserved quantity of  $\text{NO}_y$ , as well as  $\text{NO}_x$  as  $\text{NO}$ , and  $\text{NH}_x$  as  $\text{NH}_3$  + particulate ammonium. Emissions of  $\text{SO}_x$  as  $\text{SO}_2$  that include the conversion of  $\text{SO}_2$  to particulate sulfate are discussed in Rickly et al. (2022).



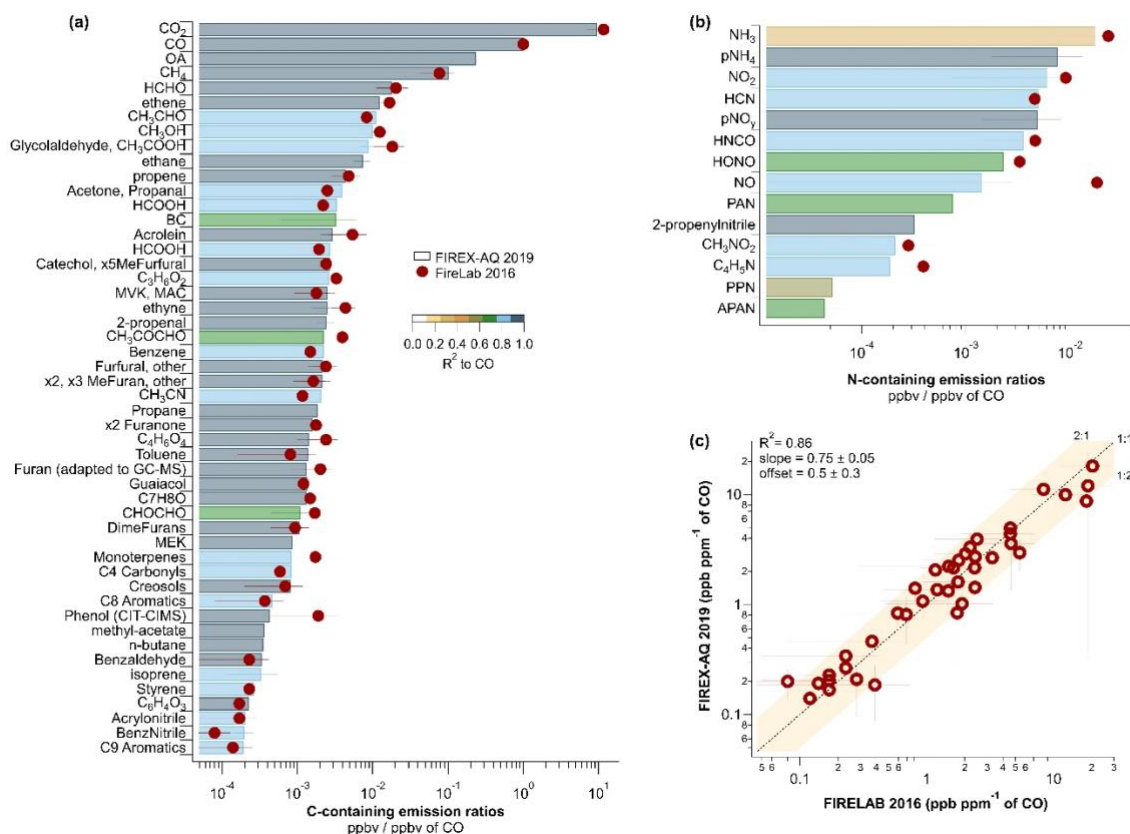
379  
380

**Figure 3:** Pie charts of carbon- and nitrogen-containing species average emission factors ( $\text{g kg}^{-1}$ ) for fresh wildfire smoke. The

381 text labels indicate compounds with only direct emissions in black, and compounds that are directly emitted and photochemically  
 382 produced in blue, and PANs that are only photochemically produced in red, indicating some oxidation even for the freshest  
 383 plumes sampled. Although HCHO and CH<sub>3</sub>CHO are C<sub>x</sub>H<sub>y</sub>O species and glycolaldehyde/acetic acid are C<sub>x</sub>H<sub>y</sub>O<sub>2</sub> species they are  
 384 separately presented due to their high abundances.

### 385 3.4 FIREX-AQ field observations compared to laboratory and field studies

386 The sum of the NMOG EFs sampled during the FIREX-AQ campaign was  $26.88 \pm 8.5 \text{ g kg}^{-1}$  ( $3\sigma$ ), in agreement  
 387 with the mean sum from western wildfires during the WE-CAN campaign of  $26.1 \pm 6.9 \text{ g kg}^{-1}$  (Permar et al., 2021),  
 388 temperate forest fires at  $23.7 \text{ g kg}^{-1}$  (Akagi et al., 2011) and  $24.55 \text{ g kg}^{-1}$  (Andreae, 2019), pine-forest understory  
 389 prescribed fires at  $27.6 \text{ g kg}^{-1}$  (Yokelson et al., 2013), FLAME-4 laboratory coniferous canopy fires at  $23.9 \text{ g kg}^{-1}$   
 390 (Stockwell et al., 2015), and FireLab laboratory measurements of various different fuel types at  $25 \text{ g kg}^{-1}$  (Koss et  
 391 al., 2018). The sum of FIREX-AQ NMOG ERs to CO on a molar basis was  $134.2 \pm 20 \text{ ppb ppm}^{-1}$ , in a similar range  
 392 as WE-CAN at  $148.3 \pm 29.6 \text{ ppb ppm}^{-1}$  and FireLab at  $144.5 \text{ ppb ppm}^{-1}$ .

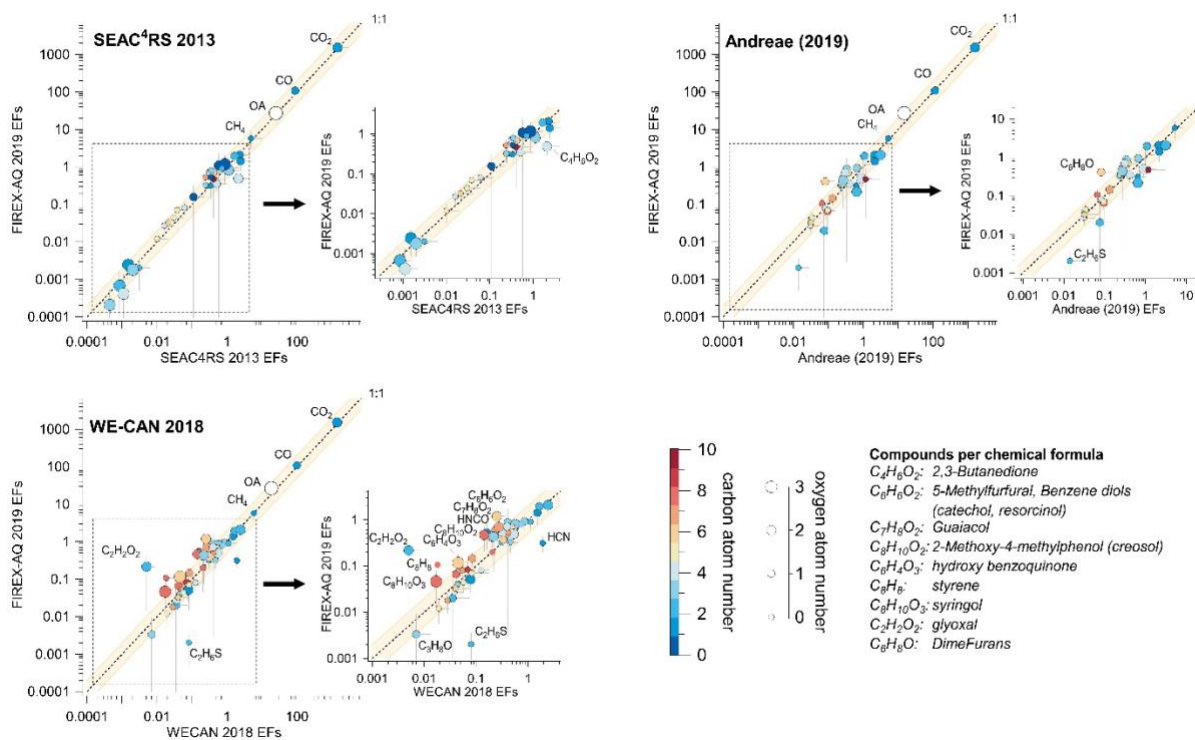


393  
 394 **Figure 4:** (a) and (b) show the emission ratios for FIREX-AQ (bars) and FireLab (circles) colored by the correlation coefficient,  
 395 and (c) direct comparison of FIREX-AQ to FireLab emission ratios for gas-phase species. Error bars in all graphs indicate the 1-  
 396 sigma standard deviation. The majority of the observations from FireLab 2016 were calculated using data from the NOAA PTR-  
 397 ToF-MS; here we use measurements from the same instrument for FIREX-AQ for more direct comparisons.

398 Figure 4 compares the ERs of C-containing and N-containing compounds (ppb ppb<sup>-1</sup> CO) with those measured at  
 399 the FireLab (Koss et al., 2018; Selimovic et al., 2018). During FIREX-AQ, all NMOGs correlated well with CO  
 400 with correlation coefficients R<sup>2</sup> above 0.75, confirming that CO could be used as a proxy for estimating NMOG  
 401 emissions close to the fire, as further discussed in Sect. 3.5. Variability in the correlations of individual species with  
 402 CO was still evident — for example, species that are both emitted and photochemically produced exhibited lower  
 403 correlation (e.g., acetic acid, acetone, and formic acid, R<sup>2</sup> = 0.75–0.85) than compounds with only primary emissions  
 404 from fires (e.g., aromatics, R<sup>2</sup> > 0.95). N-containing species were weakly correlated with CO partly due to varying  
 405 fuel N/C (Roberts et al., 2020). In addition, lower correlation of NH<sub>3</sub> could be due to variable amounts of ammonium  
 406 formation in aging smoke, or differences in instrument response times between a high volatility compound, such as  
 407 CO, compared to NH<sub>3</sub>, which may partition to the inlet and instrument walls before detection (Tomsche et al., 2023;

408 Stockwell et al., 2014) and slow the instrument response time. Low correlations are also found for HONO, which is  
 409 highly reactive and removed by photochemistry (Peng et al., 2020; Theys et al., 2020), as well as for glyoxal and  
 410 methylglyoxal, which are photochemically formed and could partition differently to the particle phase depending on  
 411 humidity (Mitsuishi et al., 2018; Ling et al., 2020). N-containing species were in good agreement except the higher  
 412 contribution of NO and particulate ammonium in Firelab and FIREX-AQ, respectively. This difference reflects the  
 413 depletion of NO and the secondary formation of particulate ammonium in field observations and promotes that fast  
 414 chemistry of reactive compounds occurred prior to the FIREX-AQ sampling. In summary, variability in post-  
 415 emission processes, fuel nitrogen, and fast photochemistry are likely important factors that contribute to the  
 416 differences in correlations between FIREX-AQ and Firelab measurements of NMOGs, NO<sub>y</sub> species, and CO.

417 While the PTR-ToF-MS is well-suited for detecting NMOGs, it is prone to fragmentation for a range of molecules,  
 418 depending on their molecular structure (Pagonis et al., 2019). For such compounds, measurement uncertainties  
 419 increase, and comparisons to previous studies that use different instrumentation become more challenging. As  
 420 outlined in Sect. 2, the NOAA PTR-ToF-MS used in this study was the same instrument as used in the FireLab three  
 421 years prior (Koss et al., 2018). This provided an important opportunity to compare field-derived emissions to  
 422 laboratory studies. FireLab average ERs were calculated by comparing similar fuel types as measured during  
 423 FIREX-AQ, including ponderosa pine, lodgepole pine, Ddouglas fir, subalpine fir, engelmann spruce, loblolly pine,  
 424 jeffrey pine, juniper, manzanita, chamise, and bear grass laboratory burns. Overall, FIREX-AQ ERs agree with those  
 425 from the FireLab within a factor of 2 for most compounds (see Fig. S3). Compounds with the largest differences  
 426 were benzonitrile with a FIREX-AQ to FireLab ratio of 2.46, ethene (1.88), CH<sub>3</sub>CN (1.77), toluene (1.71), HCOOH  
 427 (1.64), the sum of acetone and propanal (1.62), glycolaldehyde and acetic acid (0.50), monoterpenes (0.49), C<sub>4</sub>H<sub>5</sub>N  
 428 species (0.47), syringol (0.32), and ethanol (0.28).



429  
 430 **Figure 5:** Comparison of FIREX-AQ EFs to those from SEAC<sup>4</sup>RS 2013 (Liu et al., 2017), WE-CAN 2018 (Permar et al., 2021),  
 431 and the review publication by Andreae (2019). Shaded areas show differences within a factor of 2.

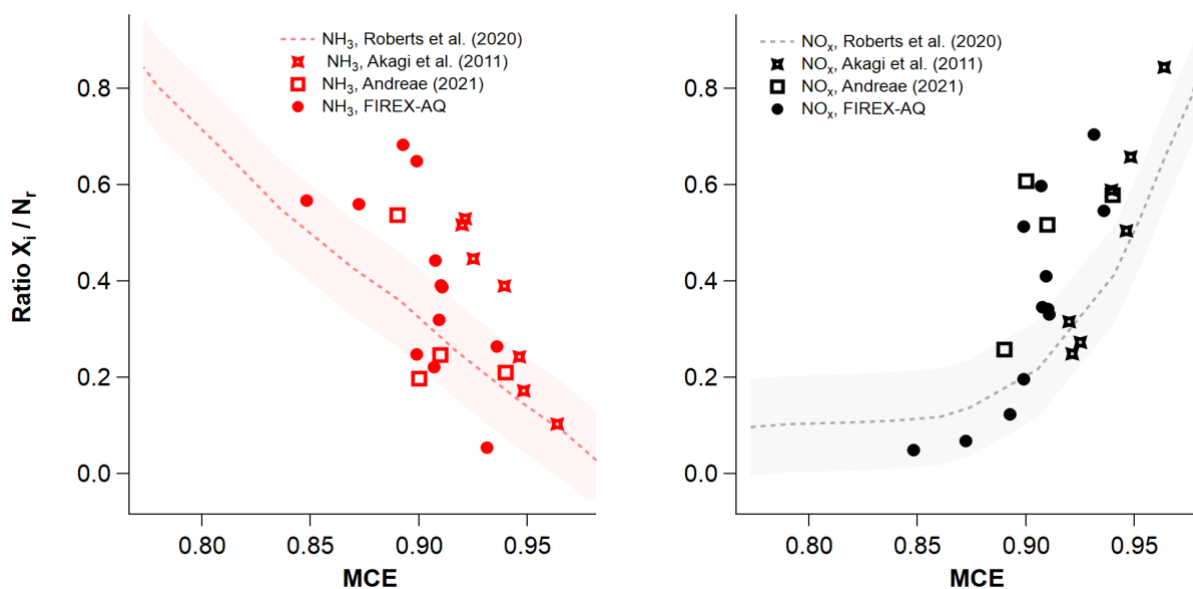
432 Figure 5 and Table S6 compare FIREX-AQ observations against field-derived wildfire EFs from SEAC<sup>4</sup>RS (Liu et  
 433 al., 2017), WE-CAN (Permar et al., 2021), and literature-average temperate forest EFs from Andreae (2019). For all  
 434 studies, the measurements agree within a factor of 2 for 83%, 87%, and 78% of the compounds reported during  
 435 SEAC<sup>4</sup>RS, WE-CAN, and the Andreae (2019) temperate forest fires average (includes SEAC<sup>4</sup>RS), respectively.  
 436 FIREX-AQ EFs were on average higher compared to previous studies. The average ratio ( $\pm 1\sigma$ ) of FIREX-AQ to  
 437 WE-CAN, SEAC<sup>4</sup>RS, and temperate forest fires from Andrea (2019) were  $1.42 \pm 0.3$ ,  $1.26 \pm 0.42$ , and  $1.24 \pm 0.36$ ,

438 respectively (see Table S6). Glyoxal and methylglyoxal were expected to have higher discrepancies due to their  
439 secondary production and RH-dependent particle-phase partitioning, but also due to the higher quantification  
440 uncertainties in the previous studies. For example, during WE-CAN (Permar et al., 2021), a PTR-ToF-MS was used  
441 to detect these compounds, which are prone to fragmentation upon ionization in the PTR-ToF-MS. Furthermore, the  
442 calculated glyoxal sensitivity used by Permar et al. (2021) was high (Stöner et al., 2016) and could therefore lead  
443 to a significant underestimation. In this study, glyoxal and methylglyoxal were measured by cavity-enhanced  
444 spectroscopy, and the uncertainties were < 5% (see Sect. 2). Furthermore, comparison of the FIREX-AQ to the  
445 FireLab EFs also measured by the same spectroscopic technique (see Fig. 4) (Zarzana et al., 2018) showed that  
446 glyoxal and methylglyoxal were in better agreement with FIREX-AQ compared to Permar et al. (2021) but still  
447 lower by 50% and 75%, respectively. Dimethyl sulfide (DMS) is a compound that originates predominantly from  
448 oceanic emissions and its fire emissions were lower for this study compared to WE-CAN and the temperate forest  
449 fire emissions average, but higher by 20% compared to the SEAC<sup>4</sup>RS EFs. FIREX-AQ monoterpenes were higher  
450 than those in WE-CAN and Firelab by a factor of 2, and lower than the temperate forest fire emissions average  
451 (Andreae 2019) by a factor of 2, which likely stems from the large variability of monoterpene emissions for different  
452 fuel types and the difficulties inherent with the large number of isomers (Hatch et al., 2017; Koss et al., 2018;  
453 Sekimoto et al., 2018). OA was 50% higher compared to WE-CAN and temperate forest fire emissions, but within  
454 10% when compared to the SEAC<sup>4</sup>RS OA emissions. Some of the OA estimates that went into the Andreae (2019)  
455 averaged OA EF value were calculated from OC with an assumed OA:OC value of 1.6, lower than the value of 1.89  
456 used in this work (Table 3); while a correction of Andreae's data is not possible since it is not transparent which  
457 studies included in that compilation are affected, this will result in a small high bias in O:C. The variability of OA  
458 EFs highlights the importance of accounting for the partitioning and aging of OA when comparing OA EFs across  
459 biomass burning campaigns given that fraction of the detected OA from wildfire plumes can be a mix of primary  
460 and secondary (Pagonis et al., 2020).

461 Focusing on the two large recent campaigns dedicated to wildfires we note that differences can occur due to natural  
462 variability with 2018 being a more intense fire season (Jin et al., 2023), but also from the different fragmentation,  
463 inlet setups, and quantification uncertainties between the instruments used. Differences between the WE-CAN and  
464 FIREX-AQ EFs for oxygenated compounds could be due to the different quantification uncertainties between the  
465 two PTR-ToF-MS instruments. For both studies and instruments, assuming similar isomer sensitivities and no  
466 fragmentation interferences, sensitivities for calibrated compounds introduced a 15% uncertainty, whereas  
467 sensitivities for uncalibrated species were estimated following theoretical methods described by Sekimoto et al.  
468 (2017), which have an uncertainty of 50%. Several reactive oxygenated compounds that have implications for NO<sub>x</sub>  
469 loss processes such as the formation of nitrophenolic compounds (Finewax et al., 2018; Decker et al., 2021) were  
470 calibrated during FIREX-AQ but only calculated during WE-CAN, such as C<sub>7</sub>H<sub>8</sub>O (o-cresol, anisol), C<sub>7</sub>H<sub>8</sub>O<sub>2</sub>  
471 (guaiacol), and C<sub>8</sub>H<sub>10</sub>O<sub>2</sub> (creosol). One mass calibrated on both instruments was C<sub>6</sub>H<sub>6</sub>O<sub>2</sub> (sum of 5-methyl-furfural,  
472 catechol, and resorcinol), but was still a factor of 5 higher during FIREX-AQ compared to WE-CAN. However, the  
473 FIREX-AQ ERs for C<sub>6</sub>H<sub>6</sub>O<sub>2</sub> agreed within 45% of the FireLab study, which used the same instrument, suggesting  
474 possible differences in fragmentation or isomer assignment between the FIREX-AQ and WE-CAN instruments.  
475 Styrene (C<sub>8</sub>H<sub>8</sub>) from FIREX-AQ (using PTR-MS) was a factor of 6 higher compared to the WE-CAN measurements  
476 (GC-MS) but agreed within 60% with SEAC<sup>4</sup>RS (GC-MS) and FireLab EFs (PTR-MS). C<sub>6</sub>H<sub>8</sub>O (sum of 2,5-  
477 dimethylfuran, 2-ethylfuran, and other C<sub>2</sub>-substituted furan isomers), C<sub>8</sub>H<sub>10</sub>O<sub>3</sub> (syringol), and C<sub>6</sub>H<sub>4</sub>O<sub>3</sub> (hydroxy  
478 benzoquinone) were quantified using estimated calibration factors during both campaigns, and therefore more  
479 uncertain, and were higher by a factor of 2–5 during FIREX-AQ. Another influencing factor for the overall higher  
480 EFs for oxygenated compounds during FIREX-AQ could be due to the optimized inlet setups to limit wall losses  
481 prior to detection for the majority of the instruments (Table 2). Various oxygenated compounds are more analytically  
482 sticky and can therefore partition to the inlet line walls prior to their detection. For example, during FIREX-AQ the  
483 NOAA PTR-ToF-MS inlet line was 1-m long and heated at 60°C to reduce condensation sinks resulting in less than  
484 1 second residence times; in Firelab (Koss et al., 2018) a longer 16 m transfer line was used at 40°C with a residence  
485 time comparable to FIREX-AQ whereas in WE-CAN (Permar et al., 2021) the smoke to drift tube time was higher  
486 (~ 2 seconds) at temperatures of 55-60°C. This could therefore contribute to differences for larger or more  
487 oxygenated NMOGs between campaigns and partly explain the overall increased EFs during FIREX-AQ.

488 Further differences between FIREX-AQ and WE-CAN may also result from the methods used to identify and  
 489 characterize young plumes. As described in Sect. 3.1, fresh plumes are identified during FIREX-AQ based on  
 490 chemical aging proxies, whereas fresh plumes identified in WE-CAN are based on physical distance downwind. For  
 491 highly reactive species, such as furans and oxygenated aromatics, strong fire-to-fire variability in OH exposure may  
 492 alter emission factors, even in smoke with similar downwind age. Figure S2 compares the FIREX-AQ and WE-  
 493 CAN field observations to the ERs obtained during the FireLab laboratory study for a variety of overlapping NMOGs  
 494 with varying reactivities towards OH radicals. Given that FireLab experiments were performed under dark and  
 495 warmer conditions in smoke aged just 5 seconds, it is expected that the more reactive compounds would show higher  
 496 ERs when compared to field observations if the sampled smoke onboard the aircraft was already aged. However,  
 497 higher ERs were observed for various compounds measured during FIREX-AQ. In contrast, when comparing WE-  
 498 CAN to FireLab ERs, the highly reactive compounds were lower although the ERs of less reactive compounds were  
 499 in good agreement. This indicates possible differences between FIREX-AQ and WE-CAN owing to variability in  
 500 chemical oxidation, which has the largest impact on highly reactive species.

501 The correlation to MCE for each species EFs was calculated for all wildfires as shown in Table S4 and compared to  
 502 the WE-CAN observations. Correlation coefficients ( $R^2$ ) during FIREX-AQ were above 0.5 for 28% of the species,  
 503 0.3–0.5 for 27% of the species, and below 0.3 for the remaining species. The lowest correlations, below 0.1, were  
 504 found for N-containing species, including particulate ammonium and  $pNO_y$ , ammonia, acetonitrile, 2-butyl nitrate,  
 505 methyl nitrate, pyrrole and butene nitrile isomers, and acrylonitrile. Nevertheless, agreement within a factor of 2  
 506 was found when compared to the slopes and  $R^2$  obtained from the WE-CAN campaign for most of the compounds.  
 507 Figure 6 shows the dependence of two N-containing species on fire MCEs for the FIREX-AQ and FireLab (Roberts  
 508 et al., 2020) studies as well as for a majority of fuel types by Akagi et al. (2011) and Andreae (2019). We report N-  
 509 containing species as a ratio to the total reactive nitrogen  $N_r$ , defined as the sum of  $NO$ ,  $NO_2$ , HONO, HCN, HCN,  
 510  $NH_3$ , other N-containing VOCs, and particle-phase nitrate and ammonium. The dotted lines and shaded regions  
 511 show FireLab parameterizations that describe how these ratios respond to changes in MCE (Roberts et al., 2020) for  
 512 one subalpine fir fire burned during FireLab whereas square and bended square markers indicate different land cover  
 513 types from Andreae (2019) and Akagi et al. (2011), respectively. It should be noted that for Akagi et al. (2011) and  
 514 Andreae (2019)  $N_r$  measurements are limited to the sum of  $NO$ ,  $NO_2$ , HONO, HCN, and  $NH_3$  and therefore the  $N_r$   
 515 could represent a lower limit. For both laboratory and field studies and independent of the fuel burnt, as MCE  
 516 increases,  $NO_x/N_r$  increases, whereas  $NH_3/N_r$  decreases. The FireLab MCE ranged from pure flaming (MCE = 0.99)  
 517 to smoldering values (MCE < 0.8), but ambient observations during FIREX-AQ were limited to MCE values ranging  
 518 from 0.85 to 0.95, which suggests both flaming and smoldering contributions to the sampled wildfire plumes.

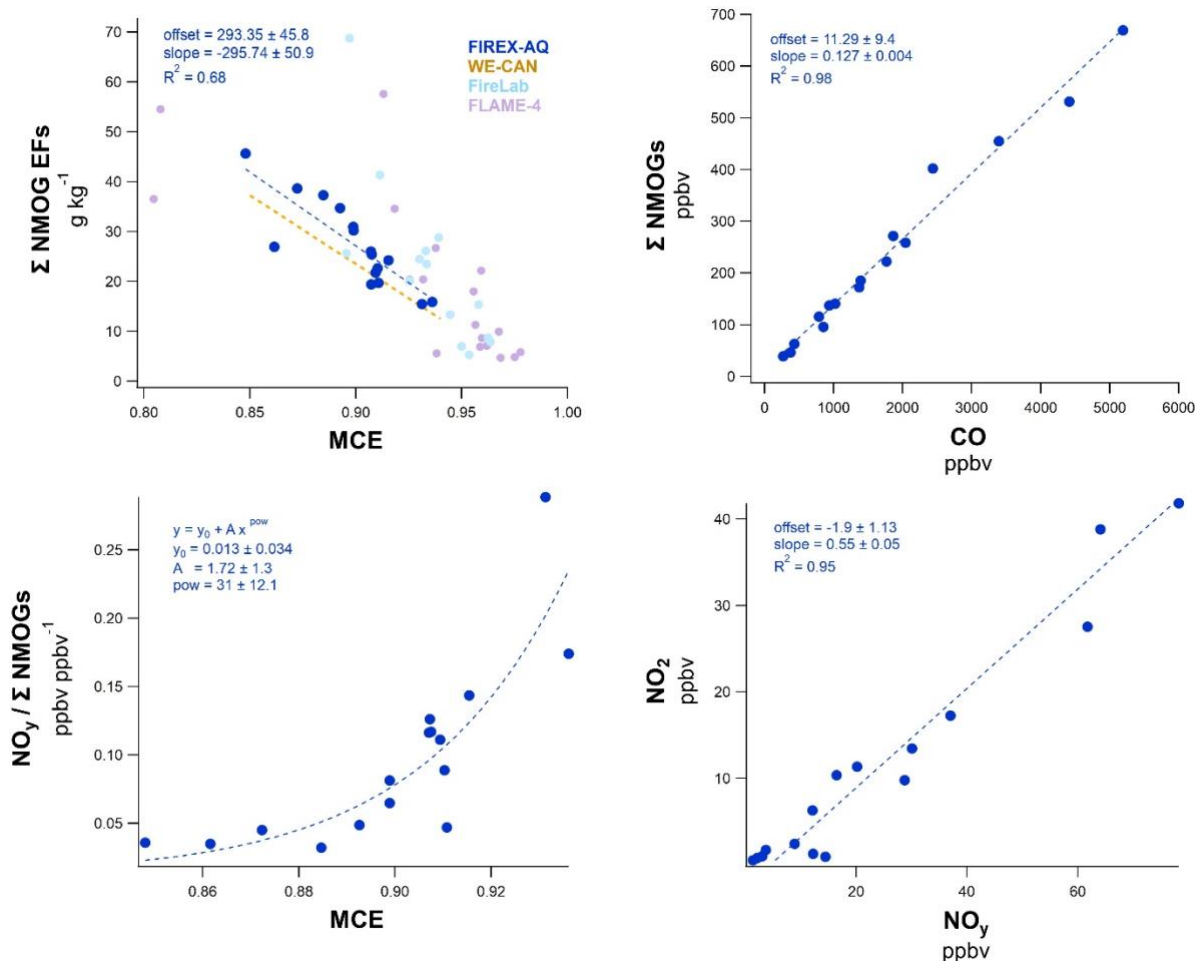


519  
 520 **Figure 6:** Ratios of two N-species to the total nitrogen,  $N_r$ , during FIREX-AQ compared to Roberts et al. (2020) based on a  
 521 subalpine fir fire burned during FireLab, and Andreae (2019) and Akagi et al. (2011) that include different land cover types.

523 The comparisons described above demonstrate that FIREX-AQ emissions agreed within a factor of 2 or better with  
524 previous laboratory and field studies for most C- and N-containing species for temperate ecosystem fuels. In the  
525 following, we relate primary wildfire emissions and emission factors to fire emissions measurable from space, e.g.,  
526 CO (e.g., Schneising et al., 2020), NO<sub>2</sub> (e.g., Martínez-Alonso et al., 2020), and BC (e.g., Konovalov et al., 2018),  
527 as well as MCE. Although current satellite retrievals for wildfire smoke can agree with airborne observations e.g.,  
528 for NO<sub>x</sub> and CO (Griffin et al., 2021; Stockwell et al., 2022), challenges in isolating the fire contribution from small  
529 or short-lived fires, as well as cloud coverage and aerosol interferences, add uncertainties to this quantification (e.g.,  
530 Jung et al., 2019; Vasilkov et al., 2021). Here, we only focus on the parameterization of wildfire plumes and promote  
531 future efforts to quantify these compounds using satellite retrievals more accurately. Satellite-retrieved  
532 concentrations of CO and NO<sub>2</sub> close to wildfires could then be used to estimate NMOG and NO<sub>y</sub> emissions and  
533 potentially better account for variability associated with fire emissions and improve modeling efforts to simplify  
534 and predict downwind formation of secondary pollutants, including ozone and secondary organic aerosol.

535 Figure 7 shows correlations between the sum of the median mixing ratios of NMOGs and NO<sub>y</sub> with MCE, CO, and  
536 NO<sub>2</sub>, where CO and NO<sub>2</sub> are two species available from satellite products that could be used as proxies for  
537 smoldering and flaming combustion (e.g., van der Velde et al., 2021; Urbanski et al., 2008), respectively. Figure 7a  
538 shows that the sum of FIREX-AQ NMOG EFs correlated with MCE with an R<sup>2</sup> of 0.68, even though many of the  
539 individual compounds are poorly correlated with MCE (Table S4). The correlation of the FIREX-AQ MCE to the  
540 sum of NMOGs was in the same range as WE-CAN, FireLab, and FLAME-4 observations. WE-CAN was  
541 consistently lower, by around 10%, which is partially due to differences in the assumed fraction of carbon employed  
542 in Eq. (1) (45.7% for WE-CAN and 50% for this study). FIREX-AQ sampled fires with lower MCEs on average  
543 than the lab experiments, with lab experiments showing highly variable EFs for MCE values below 0.9. Additional  
544 reasons for different FireLab and FLAME-4 EFs vs. MCE are discussed in detail by Permar et al. (2021) and include,  
545 (1) rapid chemistry prior to sampling, which results in the degradation of short-lived species (Fig. S2) and/or less  
546 partitioning to particles at higher lab temperatures, (2) laboratory studies may more efficiently sample smoldering  
547 combustion emissions compared to aircraft observations where residual smoldering combustion emissions might  
548 not be lofted and therefore undersampled at the aircraft altitude, and (3) laboratory MCEs are often higher than in  
549 the field due to experimental conditions, including drier fuel and more efficient burning conditions (Yokelson et al.,  
550 2013; Holder et al., 2017; Selimovic et al., 2018), whereas field MCEs are calculated from single transects through  
551 smoke plumes that likely contain a different mix of flaming vs. smoldering (Wiggins et al., 2020). Nevertheless, the  
552 good agreement between two different aircraft studies during different years and the general agreement with FireLab  
553 and FLAME-4 study averages further highlight the consistency of total NMOG correlations with MCE in wildfire  
554 emissions despite the poorer correlations of individual compounds with MCE (Table S4).





555

556 **Figure 7:** Correlation trends observed for western US wildfire emissions for (a) the sum of median NMOG EFs compared to  
 557 MCE for each wildfire. Each data point represents one fire from either FIREX-AQ, WE-CAN (Permar et al., 2021), FireLab  
 558 (Koss et al., 2018), or FLAME-4 (Stockwell et al., 2015) with the name of each FIREX-AQ fire centered on the data points. (b)  
 559 Sum of median NMOG mixing ratios plotted vs. CO, (c) ratio of median NO<sub>y</sub> species to the sum of NMOGs vs. MCE, and (d)  
 560 median NO<sub>y</sub> mixing ratios vs. the median NO<sub>2</sub> concentration. Dashed lines indicate linear fits for (a), (b), and (d), and a power  
 561 function fit for (c).

562 Figure 7b relates the sum of the median NMOG mixing ratios to the median CO mixing ratios for all the freshest  
 563 sampled wildfire plumes. CO results largely from smoldering combustion, which is the combustion process that also  
 564 produces most NMOGs. NMOGs and CO are very well correlated, with a slope of  $127 \pm 4$  (ppb ppm<sup>-1</sup>) and an R<sup>2</sup>  
 565 of 0.98, which demonstrates that total primary NMOG emissions are effectively represented by CO. Figure S4 shows  
 566 that R<sup>2</sup> values with CO for individual compounds were above 0.9 for the majority of primary NMOGs reported here,  
 567 whereas, for secondary species, the correlations were below 0.3. CO columns are retrievable from space by, e.g.,  
 568 TROPOMI (Martínez-Alonso et al., 2020) and CRiS (NASA, 2015) and can be used to derive CO emissions that  
 569 generally agree with *in situ* observations (Stockwell et al., 2022). The correlations from the FIREX-AQ  
 570 measurements and others could be used to initialize total NMOG emissions from wildfire plumes in models.

571 Quantification of N-containing species is also essential for understanding and modeling the evolution and formation  
 572 of secondary organic aerosol and ozone downwind of wildfires. Figure 7c shows the ratio of measured NO<sub>y</sub> by the  
 573 chemiluminescence instrument (see Sect. 2.1), to the sum of NMOGs in ppb ppb<sup>-1</sup>. A rapid increase in this ratio is  
 574 observed as MCE increases described by a power function fit. This increase follows the expectation that as fires  
 575 transition from smoldering to flaming conditions, MCE increases, NMOGs EFs decrease, and fuel nitrogen leads to  
 576 the formation of NO<sub>x</sub> through radical chemistry of N-containing compounds (Roberts et al., 2020). Figure 7d shows  
 577 that NO<sub>2</sub> represents a significant fraction of NO<sub>y</sub> with a slope of  $0.55 \pm 0.03$  (ppb ppb<sup>-1</sup>) and an R<sup>2</sup> of 0.95.  
 578 Furthermore, the correlation of individual N-containing species with NO<sub>2</sub> is significantly higher than their

579 correlation with CO mixing ratios (Fig. S4) promoting that NO<sub>2</sub> measurements could be used to initialize total NO<sub>y</sub>  
 580 emissions and N-species from wildfire plumes in models. Figure S5 shows additional correlations that could be used  
 581 for modeling efforts, including the correlation of NO<sub>y</sub> to CO, NO<sub>y</sub> to BC, and others.

582 These observations suggest that CO is a good proxy for species emitted from western wildfires primarily during  
 583 smoldering conditions (i.e., NMOGs), whereas NO<sub>2</sub> is a good proxy for species that are mostly emitted during  
 584 flaming conditions (i.e., mostly NO<sub>y</sub>). Thus, in addition to coupling EFs with fuel consumption to derive emissions,  
 585 we suggest future use of satellite retrievals close to the fire plume to quantify CO and NO<sub>2</sub> concentrations in order  
 586 to accurately determine EFs for all carbon and nitrogen-containing species for western US wildfire plumes as input  
 587 to models. An important assumption, especially in determining emissions of N-containing species, is that NO<sub>2</sub>  
 588 should accurately represent NO<sub>y</sub> close to the fire. However, satellite retrievals that capture truly fresh emissions very  
 589 close to the fire will be dominated by NO and HONO whereas in highly oxidized plumes NO<sub>2</sub> loss processes will  
 590 lower its overall contribution to NO<sub>y</sub>. It is therefore important to provide a range of distances where this holds true.  
 591 Coggon et al. (2022) find that for fires with highly reactive emissions, NO<sub>2</sub> represents NO<sub>y</sub> within the first 15-30  
 592 min and a distance of 10-20 km downwind of the fire assuming a wind speed 10 m/s. Current satellite retrievals for  
 593 wildfire smoke have a spatial resolution of 3.5 km × 5.5 km (Griffin et al., 2021) which would be within the above  
 594 range and high enough to represent plumes where NO<sub>2</sub> is the dominant fraction of NO<sub>y</sub>.

595 **Table 3:** Emission ratios and emission factors of organic and nitrogen compounds from wildfire plumes. In blue are multiple  
 596 isomers measured as a sum by the NOAA PTR-ToF-MS that were further speciated based on other GC-MS measurements from  
 597 FIREX-AQ (column 1 in parentheses). Here, we show the ratio of each isomer measured by GC-MS to the total PTR-ToF-MS  
 598 signal obtained in this mass.

| Compound<br><i>Isomer contribution to each mass is provided in parentheses based on the ratio of each isomer measured by GC-MS to the sum measured by PTR-ToF-MS (check Table S5)</i> | Instrument                            | Exact Mass, Da | Chemical formula/structure                   | EFs (g kg <sup>-1</sup> ) | ± σ   | ERs to CO (ppb ppm <sup>-1</sup> ) | ± σ     |
|---|---------------------------------------|----------------|--|---------------------------|-------|------------------------------------|---------|
| <b>Gas-Phase</b>  |                                       |                |  |                           |       |                                    |         |
| Carbon dioxide  | DACOM                                 | 43.99          | CO <sub>2</sub>                              | 1533.82                   | 78.06 | 9400.32                            | 2455.30 |
| Carbon monoxide   | DACOM                                 | 27.99          | CO   | 109.15                    | 22.70 | 1000.00                            | 0.00    |
| Methane   | DACOM                                 | 16.03          | CH <sub>4</sub>                              | 5.81                      | 2.68  | 91.97                              | 31.61   |
| Formaldehyde  | CAMS & ISAF                           | 30.01          | CH <sub>2</sub> O                            | 2.10                      | 0.79  | 17.92                              | 4.31    |
| Acetic acid + Glycolaldehyde  | NOAA PTR-ToF-MS for the sum           | 60.02          | C <sub>2</sub> H <sub>4</sub> O <sub>2</sub> | 2.09                      | 0.61  | 8.86                               | 1.51    |
| Acetaldehyde  | NOAA PTR-ToF-MS                       | 44.03          | C <sub>2</sub> H <sub>4</sub> O              | 1.95                      | 0.60  | 11.25                              | 1.70    |
| Ethene  | iWAS                                  | 28.03          | C <sub>2</sub> H <sub>4</sub>                | 1.52                      | 0.45  | 13.57                              | 1.97    |
| Methanol  | NOAA PTR-ToF-MS                       | 32.03          | CH <sub>4</sub> O                            | 1.42                      | 0.66  | 10.90                              | 3.21    |
| 5-Methylfurfural + Benzene diols (=Catechol, Resorcinol)  | NOAA PTR-ToF-MS for the sum           | 110.11         | C <sub>6</sub> H <sub>6</sub> O <sub>2</sub> | 1.20                      | 0.47  | 2.72                               | 0.68    |
| Acetone (78%) + Propanal (22%)  | NOAA PTR-ToF-MS (speciation by GC-MS) | 58.04          | C <sub>3</sub> H <sub>6</sub> O              | 0.93                      | 0.34  | 4.04                               | 0.84    |
| Ethane  | iWAS                                  | 30.05          | C <sub>2</sub> H <sub>6</sub>                | 0.91                      | 0.26  | 7.76                               | 1.84    |
| Methyl acetate + Ethyl formate + Hydroxyacetone   | NOAA PTR-ToF-MS for the sum           | 74.04          | C <sub>3</sub> H <sub>6</sub> O <sub>2</sub> | 0.81                      | 0.36  | 2.70                               | 0.73    |
| Propene   | iWAS                                  | 42.05          | C <sub>3</sub> H <sub>6</sub>                | 0.80                      | 0.27  | 4.80                               | 1.16    |
| MVK (38%) + Methacrolein (27%) + 2-Butenal (33%)  | NOAA PTR-ToF-MS (speciation by GC-MS) | 70.09          | C <sub>4</sub> H <sub>6</sub> O              | 0.71                      | 0.27  | 2.56                               | 0.56    |

|   |                                       |        |          |       |       |       |       |
|---|---------------------------------------|--------|----------|-------|-------|-------|-------|
| Benzene   | NOAA PTR-ToF-MS                       | 78.05  | C6H6     | 0.69  | 0.17  | 2.26  | 0.24  |
| Guaiacol (=2-Methoxyphenol)   | NOAA PTR-ToF-MS                       | 124.14 | C7H8O2   | 0.70  | 0.34  | 1.38  | 0.52  |
| Acrolein  | NOAA PTR-ToF-MS                       | 56.03  | C3H4O    | 0.88  | 0.88  | 3.73  | 2.73  |
| Methyl glyoxal  | ACES                                  | 72.06  | CH3COCHO | 0.44  | 0.36  | 1.55  | 1.23  |
| Isocyanic acid  | NOAA PTR-ToF-MS                       | 43.01  | HNCO     | 0.53  | 0.31  | 3.51  | 2.46  |
| Formic acid   | NOAA PTR-ToF-MS                       | 46.00  | HCOOH    | 0.60  | 0.43  | 3.31  | 1.95  |
| 2-Methylphenol (=o-cresol) + Anisol                                     | NOAA PTR-ToF-MS for the sum           | 108.14 | C7H8O    | 0.57  | 0.22  | 1.32  | 0.37  |
| 2(3H)-Furanone  | NOAA PTR-ToF-MS                       | 84.02  | C4H4O2   | 0.54  | 0.26  | 1.60  | 0.50  |
| HCN   | CIT-CIMS                              | 27.01  | HCN      | 0.31  | 0.12  | 3.01  | 1.08  |
| Toluene   | NOAA PTR-ToF-MS                       | 92.06  | C7H8     | 0.53  | 0.21  | 1.42  | 0.35  |
| 2,3-Butanedione + 2-Oxobutanal + 1,4-Butanedial                         | NOAA PTR-ToF-MS for the sum           | 86.04  | C4H6O2   | 0.49  | 0.20  | 1.43  | 0.37  |
| Monoterpenes  | NOAA PTR-ToF-MS                       | 136.24 | C10H16   | 0.47  | 0.43  | 0.82  | 0.65  |
| 2-Methoxy-4-methylphenol (= Creosol)                                    | NOAA PTR-ToF-MS                       | 138.16 | C8H10O2  | 0.47  | 0.26  | 0.82  | 0.36  |
| 2,5-Dimethylfuran + 2-Ethylfuran + Other unidentified organic compounds | NOAA PTR-ToF-MS for the sum           | 96.06  | C6H8O    | 0.41  | 0.16  | 1.07  | 0.27  |
| Phenol  | CIT-CIMS                              | 94.04  | C6H6O    | 0.16  | 0.05  | 0.43  | 0.13  |
| Furan   | TOGA                                  | 68.03  | C4H4O    | 0.35  | 0.13  | 1.33  | 0.40  |
| i-Butene  | iWAS                                  | 56.06  | C4H8     | 0.35  | 0.12  | 1.61  | 0.42  |
| Acetonitrile  | NOAA PTR-ToF-MS                       | 41.03  | C2H3N    | 0.32  | 0.14  | 2.04  | 0.86  |
| Propane   | iWAS                                  | 44.06  | C3H8     | 0.33  | 0.14  | 1.90  | 0.66  |
| Ethyne  | iWAS                                  | 26.02  | C2H2     | 0.30  | 0.14  | 2.90  | 0.92  |
| Glyoxal   | ACES                                  | 58.04  | CHOCHO   | 0.22  | 0.20  | 0.94  | 0.78  |
| MEK   | NOAA PTR-ToF-MS                       | 72.06  | C4H8O    | 0.24  | 0.08  | 0.84  | 0.20  |
| Ethylbenzene (7%) + m- and p-Xylenes (58%) + o-Xylene (21%)             | NOAA PTR-ToF-MS (speciation by GC-MS) | 106.17 | C8H10    | 0.08  | 0.04  | 0.18  | 0.07  |
| 2-Furfural  | TOGA                                  | 96.02  | C5H4O2   | 0.18  | 0.06  | 0.47  | 0.11  |
| Benzaldehyde  | NOAA PTR-ToF-MS                       | 106.12 | C7H6O    | 0.15  | 0.05  | 0.35  | 0.06  |
| 1-Butene  | iWAS                                  | 56.06  | C4H8     | 0.15  | 0.05  | 0.68  | 0.16  |
| Hydroxy benzoquinone  | NOAA PTR-ToF-MS                       | 124.09 | C6H4O3   | 0.12  | 0.06  | 0.23  | 0.09  |
| 2-Methylfuran   | TOGA                                  | 82.04  | C5H6O    | 0.11  | 0.04  | 0.34  | 0.10  |
| Styrene   | NOAA PTR-ToF-MS                       | 104.15 | C8H8     | 0.11  | 0.04  | 0.26  | 0.06  |
| C9 Aromatics  | NOAA PTR-ToF-MS                       | 120.19 | C9H12    | 0.084 | 0.043 | 0.178 | 0.073 |
| Naphthalene   | NOAA PTR-ToF-MS                       | 128.17 | C10H8    | 0.077 | 0.032 | 0.161 | 0.074 |
| n-Butane  | iWAS                                  | 58.08  | C4H10    | 0.082 | 0.030 | 0.368 | 0.121 |
| Benzonitrile  | NOAA PTR-ToF-MS                       | 103.04 | C7H5N    | 0.081 | 0.027 | 0.200 | 0.062 |
| 1-Pentene   | iWAS                                  | 70.08  | C5H10    | 0.073 | 0.023 | 0.268 | 0.069 |
| Benzofuran  | NOAA PTR-ToF-MS                       | 118.10 | C8H6O    | 0.067 | 0.023 | 0.143 | 0.031 |
| Butanal   | TOGA                                  | 72.06  | C4H8O    | 0.060 | 0.019 | 0.217 | 0.064 |
| Isoprene  | iWAS                                  | 68.06  | C5H8     | 0.070 | 0.055 | 0.271 | 0.203 |
| Propyne   | WAS                                   | 40.03  | C3H4     | 0.057 | 0.027 | 0.362 | 0.121 |
| 2-Methyl-1-butene   | iWAS                                  | 70.08  | C5H10    | 0.055 | 0.020 | 0.201 | 0.054 |
| Nitromethane  | NOAA PTR-ToF-MS                       | 61.02  | CH3NO2   | 0.052 | 0.025 | 0.228 | 0.116 |
| 1-Hexene  | WAS                                   | 84.09  | C6H12    | 0.049 | 0.013 | 0.151 | 0.043 |
| 2-Methylpropanal  | TOGA                                  | 72.06  | C4H8O    | 0.046 | 0.015 | 0.167 | 0.049 |

|   |   |        |                 |        |       |       |       |
|---|---|--------|-----------------|--------|-------|-------|-------|
| n-Pentane   | iWAS  | 72.09  | C5H12           | 0.044  | 0.018 | 0.159 | 0.058 |
| Acrylonitrile   | NOAA PTR-ToF-MS                             | 53.03  | C3H3N           | 0.040  | 0.011 | 0.202 | 0.073 |
| cis-2-Butene  | iWAS  | 56.06  | C4H8            | 0.013  | 0.005 | 0.045 | 0.013 |
| Syringol  | NOAA PTR-ToF-MS                             | 154.17 | C8H10O3         | 0.047  | 0.034 | 0.078 | 0.056 |
| trans-1,3-Pentadiene  | iWAS  | 68.06  | C5H8            | 0.033  | 0.015 | 0.123 | 0.044 |
| trans-2-Butene  | iWAS  | 56.06  | C4H8            | 0.037  | 0.020 | 0.166 | 0.082 |
| n-Hexane  | iWAS  | 86.11  | C6H14           | 0.033  | 0.013 | 0.099 | 0.038 |
| i-Butane  | iWAS  | 58.08  | C4H10           | 0.027  | 0.010 | 0.122 | 0.038 |
| 1-Heptene   | WAS   | 98.11  | C7H14           | 0.026  | 0.008 | 0.069 | 0.022 |
| Ethanol   | NOAA PTR-ToF-MS                             | 46.04  | C2H6O           | 0.020  | 0.055 | 0.098 | 0.273 |
| n-Nonane  | iWAS  | 128.16 | C9H20           | 0.025  | 0.010 | 0.051 | 0.020 |
| Methyl formate  | iWAS  | 60.02  | C2H4O2          | 0.020  | 0.022 | 0.089 | 0.095 |
| n-Decane  | iWAS  | 142.17 | C10H22          | 0.023  | 0.012 | 0.042 | 0.024 |
| 3-Methylfuran   | TOGA  | 82.04  | C5H6O           | 0.019  | 0.006 | 0.058 | 0.017 |
| 1-Octene  | WAS   | 112.13 | C8H16           | 0.018  | 0.005 | 0.042 | 0.013 |
| 3-Furfural  | TOGA  | 96.02  | C5H4O2          | 0.018  | 0.006 | 0.047 | 0.011 |
| trans-2-Pentene   | iWAS  | 70.08  | C5H10           | 0.018  | 0.008 | 0.065 | 0.025 |
| 2,4-Dimethylpentane   | iWAS  | 100.13 | C7H16           | 0.018  | 0.009 | 0.046 | 0.019 |
| 1-Nonene  | WAS   | 126.14 | C9H18           | 0.015  | 0.005 | 0.031 | 0.011 |
| 1-Buten-3-yne   | WAS   | 52.03  | C4H4            | 0.014  | 0.007 | 0.070 | 0.026 |
| Pyrrrole  | TOGA  | 67.04  | C4H5N           | 0.012  | 0.005 | 0.047 | 0.024 |
| i-Pentane   | iWAS  | 72.09  | C5H12           | 0.012  | 0.006 | 0.045 | 0.023 |
| cis-2-Pentene   | iWAS  | 70.08  | C5H10           | 0.013  | 0.005 | 0.045 | 0.013 |
| Butene nitrile isomers  | TOGA  | 67.04  | C4H5N           | 0.007  | 0.003 | 0.028 | 0.014 |
| 2-Methylpentane   | iWAS  | 86.11  | C6H14           | 0.007  | 0.003 | 0.020 | 0.008 |
| 1-Butyne  | WAS   | 54.05  | C4H6            | 0.006  | 0.003 | 0.030 | 0.012 |
| Methylcyclopentane  | iWAS  | 84.09  | C6H12           | 0.005  | 0.002 | 0.015 | 0.006 |
| Methylcyclohexane   | iWAS  | 98.11  | C7H14           | 0.004  | 0.002 | 0.011 | 0.006 |
| Dimethyl sulfide (50%) +<br>other unidentified organic compounds<br>(50%) | NOAA PTR-ToF-MS<br>(speciation by<br>GC-MS) | 62.02  | C2H6S           | 0.002  | 0.002 | 0.009 | 0.007 |
| 2-Butyne  | WAS   | 54.05  | C4H6            | 0.003  | 0.002 | 0.014 | 0.008 |
| Methyl nitrate  | WAS   | 77.01  | CH3NO3          | 0.002  | 0.002 | 0.008 | 0.005 |
| i-Propanol  | WAS   | 60.06  | C3H8O           | 0.003  | 0.006 | 0.015 | 0.026 |
| i-Propyl nitrate  | WAS   | 105.04 | C3H7NO3         | 0.002  | 0.001 | 0.005 | 0.002 |
| 1,3-Butadiyne   | WAS   | 50.02  | C4H2            | 0.001  | 0.001 | 0.006 | 0.002 |
| Ethyl nitrate   | WAS   | 91.03  | C2H5NO3         | 0.001  | 0.001 | 0.002 | 0.002 |
| 2-Butyl nitrate   | WAS   | 119.06 | C4H9NO3         | 0.0005 | 0.001 | 0.001 | 0.002 |
| NO <sub>y</sub>   | CL  |        | NO <sub>y</sub> |        |       | 12.10 | 7.38  |
| Nitrogen dioxide  | CL  | 46.01  | NO <sub>2</sub> | 0.93   | 0.63  | 6.05  | 5.34  |
| Nitric oxide  | CL  | 30.01  | NO              | 0.14   | 0.13  | 1.42  | 1.44  |
| Nitrous acid  | NOAA CIMS                                   | 47.00  | HONO            | 0.30   | 0.21  | 1.89  | 1.61  |
| Ammonia   | Oslo PTR-ToF-MS                             | 17.03  | NH <sub>3</sub> | 1.15   | 0.77  | 17.44 | 11.65 |

---

**Aerosol-Phase** (all units in g/kg)

|   |     |       |                               |       |       |       |       |
|---|-----|-------|-------------------------------|-------|-------|-------|-------|
| Organic aerosol<br>(OA/OC = $1.89 \pm 0.16$ ) | AMS |       | OA                            | 26.51 | 13.97 | 317.3 | 148.9 |
| Particulate nitrate                           | AMS | 62.00 | pNO <sub>y</sub>              | 0.84  | 0.3   | 7.29  | 2.69  |
| Particulate ammonium                          | AMS | 18.04 | pNH <sub>4</sub> <sup>+</sup> | 0.36  | 0.21  | 3.24  | 1.97  |
| Black carbon                                  | SP2 |       | BC                            | 0.35  | 0.32  | 3.26  | 2.69  |

### Sums

|  |                               |                                 |                 |  |      |        |       |
|--|-------------------------------|---------------------------------|-----------------|--|------|--------|-------|
| NH <sub>x</sub> as NH <sub>3</sub><br>(EF <sub>NH3</sub> + (17/18)*EF <sub>NH4</sub> ) | UIBK/UiO PTR-<br>ToF-MS + AMS | 17.03                           | NH <sub>3</sub> | NH <sub>3</sub> EFs also derived in <i>Tomsche et al. (2023)</i> |      |        |       |
| NO <sub>x</sub> as NO<br>(EF <sub>NO</sub> + (30/46)*EF <sub>NO2</sub> )               | CL                            | 30.01                           | NO              | 1.65   | 1.14 | 24.56  | 17.10 |
| SO <sub>x</sub> as SO <sub>2</sub>   | NO-LIF, AMS                   | See <i>Rickly et al. (2022)</i> |                 | 0.87   | 0.96 | 5.37   | 4.92  |
| <b>Total NMOGs emissions</b>   |                               |                                 |                 | 26.88  | 8.5  | 134.24 | 18.23 |

599

600

## Conclusions

601

We present ERs and EFs for NMOGs and nitrogen-containing compounds from nine western US wildfires and one southeastern US prescribed fire derived from data obtained aboard the NASA DC-8 during the 2019 FIREX-AQ mission. ERs and EFs were calculated for a total of 16 crosswind plume transects chosen to represent the freshest fire emissions. These transects were identified based on proxies (e.g., maleic anhydride/furan ratio) for chemical aging, which can be rapid in fire plumes.

606

We performed detailed comparisons of FIREX-AQ emissions to previous laboratory and field studies with a focus on oxygenated organic compounds that were calibrated during this mission. FIREX-AQ ERs agree within a factor of 2 to the FireLab study for most compounds, with a correlation slope of  $0.75 \pm 0.05$  and an  $R^2$  of 0.86. A comparison of the field-derived EFs from FIREX-AQ with those from SEAC<sup>4</sup>RS (Liu et al., 2017), WE-CAN (Permar et al., 2021), and temperate forest EFs from Andreae (2019) also agreed to within a factor of 2 for 87%, 83%, and 78% of the compounds, respectively. However, FIREX-AQ EFs are on average higher compared to previous studies. For compounds that agree within a factor of 2, the average ratios of FIREX-AQ to WE-CAN, SEAC<sup>4</sup>RS, and the temperate forest fire literature average are  $1.09 \pm 0.3$ ,  $1.25 \pm 0.33$ , and  $1.18 \pm 0.4$ , respectively, whereas for the remaining compounds, the ratios increase to  $2.1 \pm 1.64$ ,  $1.29 \pm 1.01$ , and  $1.32 \pm 1.23$ . We suggest that these differences could be due to differences in the fuel, quantification methods applied for each study, as well as due to differences in photochemical loss of reactive species prior to detection. Additionally, differences in fire behavior and the lofting of smoke, including variations in the mixture of flaming and smoldering combustion, could also be contributing factors. We further compare the ratio of N-containing species to the total nitrogen ( $N_i/N_T$ ) vs. MCE and find that  $NO_x/N_T$  and  $NH_3/N_T$  follow similar trends as those reported by Roberts et al. (2020).

620

We relate wildfire emissions of C- and N-containing species to CO, NO<sub>2</sub>, BC, and MCE based on correlations for use in chemical transport models. Results show that the sum of NMOG EFs correlates with MCE, with an  $R^2$  of 0.68 and a slope of  $-296 \pm 51$  g kg<sup>-1</sup>. A better correlation is observed between the sum of the median NMOG mixing ratios and median CO, with a slope of  $0.127 \pm 0.004$  (ppb ppm<sup>-1</sup>) and an  $R^2$  of 0.98. Consistent correlation of individual NMOGs to CO is also evident for the majority of NMOGs with  $R^2$  values greater than 0.9, suggesting significant potential for estimating wildfire NMOG emissions using space-based CO emissions.

626

For N-containing species, the sum of reactive nitrogen, NO<sub>y</sub>, correlates better with NO<sub>2</sub> ( $R^2 = 0.95$ , slope =  $1.74 \pm 0.1$  ppbv ppbv<sup>-1</sup>) and BC ( $R^2 = 0.88$ ) than with CO ( $R^2 = 0.7$ ) close to wildfires. Furthermore, the ratio of NO<sub>y</sub> to the sum of NMOGs increases exponentially as MCE increases. This further highlights the important influence of fire behavior, e.g., flaming vs. smoldering fire conditions on the emissions of reactive nitrogen species. Future efforts to initialize models using the above emissions parameterization could improve the representation of fire emissions in

630

631 models and their predictions on the downwind formation of secondary pollutants like ozone and secondary organic  
632 aerosol.

## 633 **Acknowledgments**

634 We would like to thank the NOAA/NASA FIREX-AQ science and aircraft operation teams. GIG, MMC, CES, MMB, IB,  
635 JMK, AL, SAM, JAN, JP, PSR, MAR, RHS, CCW, and CW were supported by the NOAA Cooperative Agreement with  
636 CIRES, NA17OAR4320101. RY and VS acknowledge NOAA grant NA16OAR4310100 and NSF grant 1748266. JL,  
637 GMW, RAH, JMS, and TFH acknowledge support from the NASA Tropospheric Composition Program and NOAA  
638 Climate Program Office's Atmospheric Chemistry, Carbon Cycle and Climate (AC4) program (NA17OAR4310004). DP,  
639 BAN, HG, PCJ, DAD, MKS, and JLJ were supported by NASA grants 80NSSC18K0630 and 80NSSC21K1451. AF was  
640 supported by NASA TCP Grant No. 80NSSC18K0628. The University of Innsbruck team was supported by the Austrian  
641 Federal Ministry for Transport, Innovation, and Technology (bmvit, FFG, ASAP). FP received funding from the European  
642 Union's Horizon 2020 research and innovation program under grant agreement No. 674911 (IMPACT EU ITN). LX, KTV,  
643 HA, JDC, and POW acknowledge NASA grant 80NSSC18K0660 and 80NSSC21K1704. This material is based upon work  
644 supported by the National Center for Atmospheric Research, sponsored by the National Science Foundation under  
645 Cooperative Agreement No. 1852977.

646

## 647 **References**

- 648 Akagi, S. K., Yokelson, R. J., Wiedinmyer, C., Alvarado, M. J., Reid, J. S., Karl, T., Crounse, J. D., and Wennberg, P.  
649 O.: Emission factors for open and domestic biomass burning for use in atmospheric models, *Atmos. Chem. Phys.*, 11,  
650 4039-4072, <https://doi.org/10.5194/acp-11-4039-2011>, 2011.
- 651  
652 Akagi, S. K., Craven, J. S., Taylor, J. W., McMeeking, G. R., Yokelson, R. J., Burling, I. R., Urbanski, S. P., Wold, C.  
653 E., Seinfeld, J. H., Coe, H., Alvarado, M. J., and Weise, D. R.: Evolution of trace gases and particles emitted by a  
654 chaparral fire in California, *Atmos. Chem. Phys.*, 12, 1397-1421, <https://doi.org/10.5194/acp-12-1397-2012>, 2012.
- 655  
656 Akagi, S. K., Burling, I. R., Mendoza, A., Johnson, T. J., Cameron, M., Griffith, D. W. T., Paton-Walsh, C., Weise, D.  
657 R., Reardon, J., and Yokelson, R. J.: Field measurements of trace gases emitted by prescribed fires in southeastern US  
658 pine forests using an open-path FTIR system, *Atmos. Chem. Phys.*, 14, 199-215, [https://doi.org/10.5194/acp-14-199-](https://doi.org/10.5194/acp-14-199-2014)  
659 [2014](https://doi.org/10.5194/acp-14-199-2014), 2014.
- 660  
661 Andreae, M. O. and Merlet, P.: Emission of trace gases and aerosols from biomass burning, *Global Biogeochem. Cy.*, 15,  
662 955-966, <https://doi.org/10.1029/2000GB001382>, 2001.
- 663  
664 Andreae, M. O.: Emission of trace gases and aerosols from biomass burning – an updated assessment, *Atmos. Chem.*  
665 *Phys.*, 19, 8523-8546, <https://doi.org/10.5194/acp-19-8523-2019>, 2019.
- 666  
667 Apel, E. C., Emmons, L. K., Karl, T., Flocke, F., Hills, A. J., Madronich, S., Lee-Taylor, J., Fried, A., Weibring, P.,  
668 Walega, J., Richter, D., Tie, X., Mauldin, L., Campos, T., Weinheimer, A., Knapp, D., Sive, B., Kleinman, L.,  
669 Springston, S., Zaveri, R., Ortega, J., Voss, P., Blake, D., Baker, A., Warneke, C., Welsh-Bon, D., de Gouw, J., Zheng,  
670 J., Zhang, R., Rudolph, J., Junkermann, W., and Riemer, D. D.: Chemical evolution of volatile organic compounds in the  
671 outflow of the Mexico City Metropolitan area, *Atmos. Chem. Phys.*, 10, 2353-2375, [https://doi.org/10.5194/acp-10-](https://doi.org/10.5194/acp-10-2353-2010)  
672 [2353-2010](https://doi.org/10.5194/acp-10-2353-2010), 2010.
- 673  
674 Apel, E. C., Hornbrook, R. S., Hills, A. J., Blake, N. J., Barth, M. C., Weinheimer, A., Cantrell, C., Rutledge, S. A.,  
675 Basarab, B., Crawford, J., Diskin, G., Homeyer, C. R., Campos, T., Flocke, F., Fried, A., Blake, D. R., Brune, W.,  
676 Pollack, I., Peischl, J., Ryerson, T., Wennberg, P. O., Crounse, J. D., Wisthaler, A., Mikoviny, T., Huey, G., Heikes, B.,  
677 O'Sullivan, D., and Riemer, D. D.: Upper tropospheric ozone production from lightning NO<sub>x</sub>-impacted convection:  
678 Smoke ingestion case study from the DC3 campaign, *J. Geophys. Res. Atmos.*, 120, 2505-2523,  
679 <https://doi.org/10.1002/2014JD022121>, 2015.
- 680  
681 Apte, J. S., Brauer, M., Cohen, A. J., Ezzati, M., and Pope, C. A.: Ambient PM<sub>2.5</sub> Reduces Global and Regional Life  
682 Expectancy, *Environ. Sci. Tech. Lett.*, 5, 546-551, <https://doi.org/10.1021/acs.estlett.8b00360>, 2018.
- 683

684 Bond, T. C., Doherty, S. J., Fahey, D. W., Forster, P. M., Bernsten, T., DeAngelo, B. J., Flanner, M. G., Ghan, S.,  
685 Kärcher, B., Koch, D., Kinne, S., Kondo, Y., Quinn, P. K., Sarofim, M. C., Schultz, M. G., Schulz, M., Venkataraman,  
686 C., Zhang, H., Zhang, S., Bellouin, N., Guttikunda, S. K., Hopke, P. K., Jacobson, M. Z., Kaiser, J. W., Klimont, Z.,  
687 Lohmann, U., Schwarz, J. P., Shindell, D., Storelvmo, T., Warren, S. G., and Zender, C. S.: Bounding the role of black  
688 carbon in the climate system: A scientific assessment, *J. Geophys. Res. Atmos.*, 118, 5380-5552,  
689 <https://doi.org/10.1002/jgrd.50171>, 2013.

690  
691 Balch, J. K., Bradley, B. A., Abatzoglou, J. T., Nagy, R. C., Fusco, E. J., and Mahood, A. L.: Human-started wildfires  
692 expand the fire niche across the United States, *P. Natl. Acad. Sci. USA*, 114, 2946,  
693 <https://doi.org/10.1073/pnas.1617394114>, 2017.

694  
695 Bourgeois, I., Peischl, J., Thompson, C. R., Aikin, K. C., Campos, T., Clark, H., Commane, R., Daube, B., Diskin, G.  
696 W., Elkins, J. W., Gao, R. S., Gaudel, A., Hints, E. J., Johnson, B. J., Kivi, R., McKain, K., Moore, F. L., Parrish, D. D.,  
697 Querel, R., Ray, E., Sánchez, R., Sweeney, C., Tarasick, D. W., Thompson, A. M., Thouret, V., Witte, J. C., Wofsy, S.  
698 C., and Ryerson, T. B.: Global-scale distribution of ozone in the remote troposphere from the ATom and HIPPO airborne  
699 field missions, *Atmos. Chem. Phys.*, 20, 10611-10635, <https://doi.org/10.5194/acp-20-10611-2020>, 2020.

700  
701 Bourgeois, I., Peischl, J., Neuman, J. A., Brown, S. S., Allen, H. M., Campuzano-Jost, P., Coggon, M. M., DiGangi, J.  
702 P., Diskin, G. S., Gilman, J. B., Gkatzelis, G. I., Guo, H., Halliday, H. A., Hanisco, T. F., Holmes, C. D., Huey, L. G.,  
703 Jimenez, J. L., Lamplugh, A. D., Lee, Y. R., Lindaas, J., Moore, R. H., Nault, B. A., Nowak, J. B., Pagonis, D., Rickly,  
704 P. S., Robinson, M. A., Rollins, A. W., Selimovic, V., St. Clair, J. M., Tanner, D., Vasquez, K. T., Veres, P. R.,  
705 Warneke, C., Wennberg, P. O., Washenfelder, R. A., Wiggins, E. B., Womack, C. C., Xu, L., Zarzana, K. J., and  
706 Ryerson, T. B.: Comparison of airborne measurements of NO, NO<sub>2</sub>, HONO, NO<sub>y</sub>, and CO during FIREX-AQ, *Atmos.*  
707 *Meas. Tech.*, 15, 4901-4930, <https://doi.org/10.5194/amt-15-4901-2022>, 2022.

708  
709 Braga, R. C., Rosenfeld, D., Weigel, R., Jurkat, T., Andreae, M. O., Wendisch, M., Pöschl, U., Voigt, C., Mahnke, C.,  
710 Borrmann, S., Albrecht, R. I., Molleker, S., Vila, D. A., Machado, L. A. T., and Grulich, L.: Further evidence for CCN  
711 aerosol concentrations determining the height of warm rain and ice initiation in convective clouds over the Amazon  
712 basin, *Atmos. Chem. Phys.*, 17, 14433-14456, <https://doi.org/10.5194/acp-17-14433-2017>, 2017.

713  
714 Brey, S. J. and Fischer, E. V.: Smoke in the City: How Often and Where Does Smoke Impact Summertime Ozone in the  
715 United States? *Environ. Sci. Technol.*, 50, <https://doi.org/10.1021/acs.est.5b05218>, 2015.

716  
717 Canagaratna, M. R., Jayne, J. T., Jimenez, J. L., Allan, J. D., Alfarra, M. R., Zhang, Q., Onasch, T. B., Drewnick, F.,  
718 Coe, H., Middlebrook, A., Delia, A., Williams, L. R., Trimborn, A. M., Northway, M. J., DeCarlo, P. F., Kolb, C. E.,  
719 Davidovits, P., and Worsnop, D. R.: Chemical and microphysical characterization of ambient aerosols with the aerodyne  
720 aerosol mass spectrometer, *Mass Spectrom. Rev.*, 26, 185-222, <https://doi.org/10.1002/mas.20115>, 2007.

721  
722 Cazorla, M., Wolfe, G. M., Bailey, S. A., Swanson, A. K., Arkinson, H. L., and Hanisco, T. F.: A new airborne laser-  
723 induced fluorescence instrument for in situ detection of formaldehyde throughout the troposphere and lower stratosphere,  
724 *Atmos. Meas. Tech.*, 8, 541-552, <https://doi.org/10.5194/amt-8-541-2015>, 2015.

725  
726 Cecchini, M. A., Machado, L. A. T., Andreae, M. O., Martin, S. T., Albrecht, R. I., Artaxo, P., Barbosa, H. M. J.,  
727 Borrmann, S., Fütterer, D., Jurkat, T., Mahnke, C., Minikin, A., Molleker, S., Pöhlker, M. L., Pöschl, U., Rosenfeld, D.,  
728 Voigt, C., Weinzierl, B., and Wendisch, M.: Sensitivities of Amazonian clouds to aerosols and updraft speed, *Atmos.*  
729 *Chem. Phys.*, 17, <https://doi.org/10.5194/acp-17-10037-2017>, 2017.

730  
731 Cochrane, M. A., Moran, C. J., Wimberly, M. C., Baer, A. D., Finney, M. A., Beckendorf, K. L., Eidenshink, J., and  
732 Zhu, Z.: Estimation of wildfire size and risk changes due to fuels treatments, *Int. J. Wildland Fire*, 21, 357-367,  
733 <https://doi.org/10.1071/WF11079>, 2012.

734  
735 Coggon, M. M., Lim, C. Y., Koss, A. R., Sekimoto, K., Yuan, B., Gilman, J. B., Hagan, D. H., Selimovic, V., Zarzana,  
736 K. J., Brown, S. S., Roberts, J. M., Müller, M., Yokelson, R., Wisthaler, A., Krechmer, J. E., Jimenez, J. L., Cappa, C.,  
737 Kroll, J. H., de Gouw, J., and Warneke, C.: OH chemistry of non-methane organic gases (NMOGs) emitted from  
738 laboratory and ambient biomass burning smoke: evaluating the influence of furans and oxygenated aromatics on ozone  
739 and secondary NMOG formation, *Atmos. Chem. Phys.*, 19, 14875-14899, <https://doi.org/10.5194/acp-19-14875-2019>,  
740 2019.

741  
742 Colman, J. J., Swanson, A. L., Meinardi, S., Sive, B. C., Blake, D. R., and Rowland, F. S.: Description of the Analysis of  
743 a Wide Range of Volatile Organic Compounds in Whole Air Samples Collected during PEM-Tropics A and B, *Anal.*  
744 *Chem.*, 73, 3723-3731, <https://doi.org/10.1021/ac010027g>, 2001.

745

746 Crouse, J. D., McKinney, K. A., Kwan, A. J., and Wennberg, P. O.: Measurement of Gas-Phase Hydroperoxides by  
747 Chemical Ionization Mass Spectrometry, *Anal. Chem.*, 78, 6726-6732, <https://doi.org/10.1021/ac0604235>, 2006.

748

749 Crutzen, P. J. and Andreae, M. O.: Biomass Burning in the Tropics: Impact on Atmospheric Chemistry and  
750 Biogeochemical Cycles, *Science*, 250, 1669, <https://doi.org/10.1126/science.250.4988.1669>, 1990.

751

752 Day, D. A., Campuzano-Jost, P., Nault, B. A., Palm, B. B., Hu, W., Guo, H., Wooldridge, P. J., Cohen, R. C., Docherty,  
753 K. S., Huffman, J. A., de Sá, S. S., Martin, S. T., and Jimenez, J. L.: A Systematic Re-evaluation of Methods for  
754 Quantification of Bulk Particle-phase Organic Nitrates Using Real-time Aerosol Mass Spectrometry, *Atmos. Meas.*  
755 *Tech.*, 15, 459–483, <https://doi.org/10.5194/amt-15-459-2022>, 2022.

756

757 Decker, Z. C. J., Robinson, M. A., Barsanti, K. C., Bourgeois, I., Coggon, M. M., DiGangi, J. P., Diskin, G. S., Flocke,  
758 F. M., Franchin, A., Fredrickson, C. D., Hall, S. R., Halliday, H., Holmes, C. D., Huey, L. G., Lee, Y. R., Lindaas, J.,  
759 Middlebrook, A. M., Montzka, D. D., Moore, R. H., Neuman, J. A., Nowak, J. B., Palm, B. B., Peischl, J., Piel, F.,  
760 Rickly, P. S., Rollins, A. W., Ryerson, T. B., Schwantes, R. H., Sekimoto, K., Thornhill, L., Thornton, J. A., Tyndall, G.  
761 S., Ullmann, K., Van Rooy, P., Veres, P. R., Warneke, C., Washenfelder, R. A., Weinheimer, A. J., Wiggins, E.,  
762 Winstead, E., Wisthaler, A., Womack, C., and Brown, S. S.: Nighttime and daytime dark oxidation chemistry in wildfire  
763 plumes: an observation and model analysis of FIREX-AQ aircraft data, *Atmos. Chem. Phys.*, 21, 16293–16317,  
764 <https://doi.org/10.5194/acp-21-16293-2021>, 2021.

765

766 Dennekamp, M., Straney, L. D., Erbas, B., Abramson, M. J., Keywood, M., Smith, K., Sim, M. R., Glass, D. C., Del  
767 Monaco, A., Haikerwal, A., and Tonkin, A. M.: Forest Fire Smoke Exposures and Out-of-Hospital Cardiac Arrests in  
768 Melbourne, Australia: A Case-Crossover Study, *Environ. Health Persp.*, 123, 959-964,  
769 <https://doi.org/10.1289/ehp.1408436>, 2015.

770

771 Finewax, Z., de Gouw, J. A., and Ziemann, P. J.: Identification and Quantification of 4-Nitrocatechol Formed from OH  
772 and NO<sub>3</sub> Radical-Initiated Reactions of Catechol in Air in the Presence of NO<sub>x</sub>: Implications for Secondary Organic  
773 Aerosol Formation from Biomass Burning, *Environ. Sci. Technol.*, 52, 1981–1989,  
774 <https://doi.org/10.1021/acs.est.7b05864>, 2018.

775

776 Flannigan, M., Cantin, A. S., de Groot, W. J., Wotton, M., Newbery, A., and Gowman, L. M.: Global wildland fire  
777 season severity in the 21st century, *For. Ecol. Manag.*, 294, 54-61, <https://doi.org/10.1016/j.foreco.2012.10.022>, 2013.

778

779 Fried, A., Walega, J., Weibring, P., Richter, D., Simpson, I. J., Blake, D. R., Blake, N. J., Meinardi, S., Barletta, B.  
780 Hughes, S. C., Crawford, J. H., Diskin, G. Barrick, J., Hair, J., Fenn, M., Wisthaler, A., Mikoviny, T., Woo, J.-H. Park,  
781 M., Kim, J., Min, K.-E., Jeong, S., Wennberg, P. O., Kim, M. J., Crouse, J. D., Teng, A. P., Bennett, R., Yang-Martin,  
782 M., Shook, M. A., Huey, G., Tanner, D., Knote, C., Kim, J., Park, R., and Brune, W.: Airborne formaldehyde and  
783 volatile organic compound measurements over the Daesan petrochemical complex on Korea's northwest coast during the  
784 Korea-United States Air Quality study: Estimation of emission fluxes and effects on air quality, *Elem. Sci. Anth.*, 8:1,  
785 <https://doi.org/10.1525/elementa.2020.121>, 2020.

786

787 Gilman, J. B., Lerner, B. M., Kuster, W. C., Goldan, P. D., Warneke, C., Veres, P. R., Roberts, J. M., de Gouw, J. A.,  
788 Burling, I. R., and Yokelson, R. J.: Biomass burning emissions and potential air quality impacts of volatile organic  
789 compounds and other trace gases from fuels common in the US, *Atmos. Chem. Phys.*, 15, 13915-13938,  
790 <https://doi.org/10.5194/acp-15-13915-2015>, 2015.

791

792 Griffin, D., McLinden, C. A., Dammers, E., Adams, C., Stockwell, C. E., Warneke, C., Bourgeois, I., Peischl, J.,  
793 Ryerson, T. B., Zarzana, K. J., Rowe, J. P., Volkamer, R., Knote, C., Kille, N., Koenig, T. K., Lee, C. F., Rollins, D.,  
794 Rickly, P. S., Chen, J., Fehr, L., Bourassa, A., Degenstein, D., Hayden, K., Mihele, C., Wren, S. N., Liggio, J.,  
795 Akingunola, A., and Makar, P.: Biomass burning nitrogen dioxide emissions derived from space with TROPOMI:  
796 methodology and validation, *Atmos. Meas. Tech.*, 14, 7929-7957, <https://doi.org/10.5194/amt-14-7929-2021>, 2021.

797

798 Guo, H., Campuzano-Jost, P., Nault, B. A., Day, D. A., Schroder, J. C., Kim, D., Dibb, J. E., Dollner, M., Weinzierl, B.,  
799 and Jimenez, J. L.: The importance of size ranges in aerosol instrument intercomparisons: a case study for the  
800 Atmospheric Tomography Mission, *Atmos. Meas. Tech.*, 14, 3631-3655, <https://doi.org/10.5194/amt-14-3631-2021>,  
801 2021.

802

803 Hamilton, D. S., Hantson, S., Scott, C. E., Kaplan, J. O., Pringle, K. J., Nieradzik, L. P., Rap, A., Folberth, G. A.,  
804 Spracklen, D. V., and Carslaw, K. S.: Reassessment of pre-industrial fire emissions strongly affects anthropogenic  
805 aerosol forcing, *Nat. Commun.*, 9, 3182, <https://doi.org/10.1038/s41467-018-05592-9>, 2018.



806 Hatch, L. E., Yokelson, R. J., Stockwell, C. E., Veres, P. R., Simpson, I. J., Blake, D. R., Orlando, J. J., and Barsanti, K.  
807 C.: Multi-instrument comparison and compilation of non-methane organic gas emissions from biomass burning and  
808 implications for smoke-derived secondary organic aerosol precursors, *Atmos. Chem. Phys.*, 17, 1471-1489,  
809 <https://doi.org/10.5194/acp-17-1471-2017>, 2017.  
810  
811 Hodshire, A. L., Bian, Q., Ramnarine, E., Lonsdale, C. R., Alvarado, M. J., Kreidenweis, S. M., Jathar, S. H., and Pierce,  
812 J. R.: More Than Emissions and Chemistry: Fire Size, Dilution, and Background Aerosol Also Greatly Influence Near-  
813 Field Biomass Burning Aerosol Aging, *J. Geophys. Res. Atmos.*, 124, 5589-5611,  
814 <https://doi.org/10.1029/2018JD029674>, 2019.  
815  
816 Holder, A. L., Gullett, B. K., Urbanski, S. P., Elleman, R., O'Neill, S., Tabor, D., Mitchell, W., and Baker, K. R.:  
817 Emissions from prescribed burning of agricultural fields in the Pacific Northwest, *Atmos. Environ.*, 166, 22-33,  
818 <https://doi.org/10.1016/j.atmosenv.2017.06.043>, 2017.  
819  
820 Holmes, C. D., Fite, C., Agastra, A., Schwarz, J. P., Yokelson, R. J., Bui, T. V., and Peterson, D. A.: Critical evaluation  
821 of smoke age inferred from different methods during FIREX-AQ,  
822 <https://ui.adsabs.harvard.edu/abs/2020AGUFMA225.0010H>, 2020.  
823  
824 Isaacman-VanWertz, G., Sueper, D. T., Aikin, K. C., Lerner, B. M., Gilman, J. B., de Gouw, J. A., Worsnop, D. R., and  
825 Goldstein, A. H.: Automated single-ion peak fitting as an efficient approach for analyzing complex chromatographic  
826 data, *J. Chromatogr. A*, 1529, 81-92, <https://doi.org/10.1016/j.chroma.2017.11.005>, 2017.  
827  
828 Johnston, F. H., Henderson, S. B., Chen, Y., Randerson, J. T., Marlier, M., DeFries, R. S., Kinney, P., Bowman, D. M. J.  
829 S., and Brauer, M.: Estimated Global Mortality Attributable to Smoke from Landscape Fires, *Environ. Health Persp.*,  
830 120, 695-701, <https://doi.org/10.1289/ehp.1104422>, 2012.  
831  
832 Jung, Y., González Abad, G., Nowlan, C. R., Chance, K., Liu, X., Torres, O., and Ahn, C.: Explicit Aerosol Correction  
833 of OMI Formaldehyde Retrievals, *Earth Space Sci.*, 6, 2087-2105, <https://doi.org/10.1029/2019EA000702>, 2019.  
834  
835 Keywood, M., Kanakidou, M., Stohl, A., Dentener, F., Grassi, G., Meyer, C. P., Torseth, K., Edwards, D., Thompson, A.  
836 M., Lohmann, U., and Burrows, J.: Fire in the Air: Biomass Burning Impacts in a Changing Climate, *Crit. Rev. i Environ.*  
837 *Sci. Technol.*, 43, 40-83, <https://doi.org/10.1080/10643389.2011.604248>, 2013.  
838  
839 Kloster, S., Mahowald, N. M., Randerson, J. T., Thornton, P. E., Hoffman, F. M., Levis, S., Lawrence, P. J., Feddema, J.  
840 J., Oleson, K. W., and Lawrence, D. M.: Fire dynamics during the 20th century simulated by the Community Land  
841 Model, *Biogeosciences*, 7, 1877-1902, <https://doi.org/10.5194/bg-7-1877-2010>, 2010.  
842  
843 Knorr, W., Dentener, F., Lamarque, J.-F., Jiang, L., and Arneeth, A.: Wildfire air pollution hazard during the 21st century,  
844 *Atmos. Chem. Phys.*, 17, 9223-9236, <https://doi.org/10.5194/acp-17-9223-2017>, 2017.  
845  
846 Kodros, J. K., Papanastasiou, D. K., Paglione, M., Masiol, M., Squizzato, S., Florou, K., Skyllakou, K., Kaltsonoudis, C.,  
847 Nenes, A., and Pandis, S. N.: Rapid dark aging of biomass burning as an overlooked source of oxidized organic aerosol,  
848 *P. Natl. Acad. Sci. USA*, 117, 33028, <https://doi.org/10.1073/pnas.2010365117>, 2020.  
849  
850 Konovalov, I. B., Lvova, D. A., Beekmann, M., Jethva, H., Mikhailov, E. F., Paris, J. D., Belan, B. D., Kozlov, V. S.,  
851 Ciais, P., and Andreae, M. O.: Estimation of black carbon emissions from Siberian fires using satellite observations of  
852 absorption and extinction optical depths, *Atmos. Chem. Phys.*, 18, 14889-14924, [https://doi.org/10.5194/acp-18-14889-](https://doi.org/10.5194/acp-18-14889-2018)  
853 [2018](https://doi.org/10.5194/acp-18-14889-2018), 2018.  
854  
855 Koss, A. R., Sekimoto, K., Gilman, J. B., Selimovic, V., Coggon, M. M., Zarzana, K. J., Yuan, B., Lerner, B. M., Brown,  
856 S. S., Jimenez, J. L., Krechmer, J., Roberts, J. M., Warneke, C., Yokelson, R. J., and de Gouw, J.: Non-methane organic  
857 gas emissions from biomass burning: identification, quantification, and emission factors from PTR-ToF during the  
858 FIREX 2016 laboratory experiment, *Atmos. Chem. Phys.*, 18, 3299-3319, <https://doi.org/10.5194/acp-18-3299-2018>,  
859 2018.  
860  
861 Le Quéré, C., Andrew, R. M., Friedlingstein, P., Sitch, S., Hauck, J., Pongratz, J., Pickers, P. A., Korsbakken, J. I.,  
862 Peters, G. P., Canadell, J. G., Arneeth, A., Arora, V. K., Barbero, L., Bastos, A., Bopp, L., Chevallier, F., Chini, L. P.,  
863 Ciais, P., Doney, S. C., Gkritzalis, T., Goll, D. S., Harris, I., Haverd, V., Hoffman, F. M., Hoppema, M., Houghton, R.  
864 A., Hurtt, G., Ilyina, T., Jain, A. K., Johannessen, T., Jones, C. D., Kato, E., Keeling, R. F., Goldewijk, K. K.,  
865 Landschützer, P., Lefèvre, N., Lienert, S., Liu, Z., Lombardozzi, D., Metzl, N., Munro, D. R., Nabel, J. E. M. S.,  
866

867 Nakaoka, S., Neill, C., Olsen, A., Ono, T., Patra, P., Peregon, A., Peters, W., Peylin, P., Pfeil, B., Pierrot, D., Poulter, B.,  
868 Rehder, G., Resplandy, L., Robertson, E., Rocher, M., Rödenbeck, C., Schuster, U., Schwinger, J., Séférian, R.,  
869 Skjelvan, I., Steinhoff, T., Sutton, A., Tans, P. P., Tian, H., Tilbrook, B., Tubiello, F. N., van der Laan-Luijkx, I. T., van  
870 der Werf, G. R., Viovy, N., Walker, A. P., Wiltshire, A. J., Wright, R., Zaehle, S., and Zheng, B.: Global Carbon Budget  
871 2018, *Earth Syst. Sci. Data*, 10, 2141-2194, <https://doi.org/10.5194/essd-10-2141-2018>, 2018.  
872  
873 Lerner, B. M., Gilman, J. B., Aikin, K. C., Atlas, E. L., Goldan, P. D., Graus, M., Hendershot, R., Isaacman-VanWertz,  
874 G. A., Koss, A., Kuster, W. C., Lueb, R. A., McLaughlin, R. J., Peischl, J., Sueper, D., Ryerson, T. B., Tokarek, T. W.,  
875 Warneke, C., Yuan, B., and de Gouw, J. A.: An improved, automated whole air sampler and gas chromatography mass  
876 spectrometry analysis system for volatile organic compounds in the atmosphere, *Atmos. Meas. Tech.*, 10, 291-313,  
877 <https://doi.org/10.5194/amt-10-291-2017>, 2017.  
878  
879 Liao, J., Wolfe, G. M., Hannun, R. A., St. Clair, J. M., Hanisco, T. F., Gilman, J. B., Lamplugh, A., Selimovic, V.,  
880 Diskin, G. S., Nowak, J. B., Halliday, H. S., DiGangi, J. P., Hall, S. R., Ullmann, K., Holmes, C. D., Fite, C. H., Agastra,  
881 A., Ryerson, T. B., Peischl, J., Bourgeois, I., Warneke, C., Coggon, M. M., Gkatzelis, G. I., Sekimoto, K., Fried, A.,  
882 Richter, D., Weibring, P., Apel, E. C., Hornbrook, R. S., Brown, S. S., Womack, C. C., Robinson, M. A., Washenfelder,  
883 R. A., Veres, P. R., and Neuman, J. A.: Formaldehyde evolution in U.S. wildfire plumes during the Fire Influence on  
884 Regional to Global Environments and Air Quality experiment (FIREX-AQ), *Atmos. Chem. Phys.*, 21, 18319–18331,  
885 <https://doi.org/10.5194/acp-21-18319-2021>, 2021.  
886  
887 Lindaas, J., Pollack, I. B., Garofalo, L. A., Pothier, M. A., Farmer, D. K., Kreidenweis, S. M., Campos, T. L., Flocke, F.,  
888 Weinheimer, A. J., Montzka, D. D., Tyndall, G. S., Palm, B. B., Peng, Q., Thornton, J. A., Permar, W., Wielgasz, C., Hu,  
889 L., Ottmar, R. D., Restaino, J. C., Hudak, A. T., Ku, I. T., Zhou, Y., Sive, B. C., Sullivan, A., Collett Jr, J. L., and  
890 Fischer, E. V.: Emissions of Reactive Nitrogen From Western U.S. Wildfires During Summer 2018, *J. Geophys. Res.*  
891 *Atmos.*, 126, e2020JD032657, <https://doi.org/10.1029/2020JD032657>, 2021.  
892  
893 Ling, Z., Xie, Q., Shao, M., Wang, Z., Wang, T., Guo, H., and Wang, X.: Formation and sink of glyoxal and  
894 methylglyoxal in a polluted subtropical environment: observation-based photochemical analysis and impact evaluation,  
895 *Atmos. Chem. Phys.*, 20, 11451-11467, <https://doi.org/10.5194/acp-20-11451-2020>, 2020.  
896  
897 Liu, X., Huey, L. G., Yokelson, R. J., Selimovic, V., Simpson, I. J., Müller, M., Jimenez, J. L., Campuzano-Jost, P.,  
898 Beyersdorf, A. J., Blake, D. R., Butterfield, Z., Choi, Y., Crouse, J. D., Day, D. A., Diskin, G. S., Dubey, M. K.,  
899 Fortner, E., Hanisco, T. F., Hu, W., King, L. E., Kleinman, L., Meinardi, S., Mikoviny, T., Onasch, T. B., Palm, B. B.,  
900 Peischl, J., Pollack, I. B., Ryerson, T. B., Sachse, G. W., Sedlacek, A. J., Shilling, J. E., Springston, S., St. Clair, J. M.,  
901 Tanner, D. J., Teng, A. P., Wennberg, P. O., Wisthaler, A., and Wolfe, G. M.: Airborne measurements of western U.S.  
902 wildfire emissions: Comparison with prescribed burning and air quality implications, *J. Geophys. Res. Atmos.*, 122,  
903 6108-6129, <https://doi.org/10.1002/2016JD026315>, 2017.  
904  
905 Mann, M. L., Batllori, E., Moritz, M. A., Waller, E. K., Berck, P., Flint, A. L., Flint, L. E., and Dolfi, E.: Incorporating  
906 Anthropogenic Influences into Fire Probability Models: Effects of Human Activity and Climate Change on Fire Activity  
907 in California, *PLOS ONE*, 11, e0153589, <https://doi.org/10.1371/journal.pone.0153589>, 2016.  
908  
909 Martínez-Alonso, S., Deeter, M., Worden, H., Borsdorff, T., Aben, I., Commane, R., Daube, B., Francis, G., George, M.,  
910 Landgraf, J., Mao, D., McKain, K., and Wofsy, S.: 1.5 years of TROPOMI CO measurements: comparisons to MOPITT  
911 and ATom, *Atmos. Meas. Tech.*, 13, 4841-4864, <https://doi.org/10.5194/amt-13-4841-2020>, 2020.  
912  
913 Min, K. E., Washenfelder, R. A., Dubé, W. P., Langford, A. O., Edwards, P. M., Zarzana, K. J., Stutz, J., Lu, K., Rohrer,  
914 F., Zhang, Y., and Brown, S. S.: A broadband cavity enhanced absorption spectrometer for aircraft measurements of  
915 glyoxal, methylglyoxal, nitrous acid, nitrogen dioxide, and water vapor, *Atmos. Meas. Tech.*, 9, 423-440,  
916 <https://doi.org/10.5194/amt-9-423-2016>, 2016.  
917  
918 Mitsuishi, K., Iwasaki, M., Takeuchi, M., Okochi, H., Kato, S., Ohira, S.-I., and Toda, K.: Diurnal Variations in  
919 Partitioning of Atmospheric Glyoxal and Methylglyoxal between Gas and Particles at the Ground Level and in the Free  
920 Troposphere, *ACS Earth Space Chem.*, 2, 915-924, <https://doi.org/10.1021/acsearthspacechem.8b00037>, 2018.  
921  
922 Moritz, M. A., Parisien, M.-A., Batllori, E., Krawchuk, M. A., Van Dorn, J., Ganz, D. J., and Hayhoe, K.: Climate  
923 change and disruptions to global fire activity, *Ecosphere*, 3, 49, <https://doi.org/10.1890/ES11-00345.1>, 2012.  
924  
925 Mouat, A. P., Paton-Walsh, C., Simmons, J. B., Ramirez-Gamboa, J., Griffith, D. W. T., and Kaiser, J.: Measurement  
926 report: Observations of long-lived volatile organic compounds from the 2019-2020 Australian wildfires during the  
927 COALA campaign, *Atmos. Chem. Phys.*, 2022, 22, 11033-11047, <https://doi.org/10.5194/acp-22-11033-2022>, 2022..

- 929 Müller, M., Anderson, B. E., Beyersdorf, A. J., Crawford, J. H., Diskin, G. S., Eichler, P., Fried, A., Keutsch, F. N.,  
 930 Mikoviny, T., Thornhill, K. L., Walega, J. G., Weinheimer, A. J., Yang, M., Yokelson, R. J., and Wisthaler, A.: In situ  
 931 measurements and modeling of reactive trace gases in a small biomass burning plume, *Atmos. Chem. Phys.*, 16, 3813-  
 932 3824, <https://doi.org/10.5194/acp-16-3813-2016>, 2016.
- 933  
 934 NASA airborne science data for atmospheric composition, <https://doi.org/10.5067/suborbital/fireaq2019/data001>, 2019.
- 935  
 936 National Interagency Fire Center; Internetseite vom 24.10.2015: Total Wildland Fires and Acres (1960-2009).  
 937 [http://www.nifc.gov/fireInfo/fireInfo\\_stats\\_totalFires.html](http://www.nifc.gov/fireInfo/fireInfo_stats_totalFires.html), <https://www.nifc.gov/fire-information/statistics/wildfires>,  
 938 <https://www.nifc.gov/fire-information/statistics/prescribed-fire>
- 939  
 940 Olivier, J. G. J., Van Aardenne, J. A., Dentener, F. J., Pagliari, V., Ganzeveld, L. N., and Peters, J. A. H. W.: Recent  
 941 trends in global greenhouse gas emissions: regional trends 1970–2000 and spatial distribution of key sources in 2000,  
 942 *Environmental Sciences*, 2, 81-99, <https://doi.org/10.1080/15693430500400345>, 2005.
- 943  
 944 Pagonis, D., Sekimoto, K. and de Gouw, J. A.: A library of proton-transfer reactions of H<sub>3</sub>O<sup>+</sup> ions used for trace gas  
 945 detection, *J. Am. Soc. Mass Spectrom.*, 30, 1330–1335, <https://doi.org/10.1007/s13361-019-02209-3>, 2019.
- 946  
 947 Pagonis, D., Campuzano-Jost, P., Guo, H., Day, D. A., Schueneman, M., Nault, B. A., Brown, W., Laskin, A., Siemens,  
 948 K. S. A., Coggon, M. M., DiGangi, J. P., Diskin, G. S., Fenn, M. A., Gkatzelis, G., Hair, J. W., Halliday, H. S., Katich, J.  
 949 M., Nowak, J. B., Perring, A. E., Saide, P. E., Sekimoto, K., Shingler, T. J., Thapa, L., Warneke, C., and Jimenez, J. L.:  
 950 Chemical Aging of Biomass Burning Organic Aerosol: Insight from Fast Near-Molecular Measurements, December 01,  
 951 2020.
- 952  
 953 Pagonis, D., Campuzano-Jost, P., Guo, H., Day, D. A., Schueneman, M. K., Brown, W. L., Nault, B. A., Stark, H.,  
 954 Siemens, K., Laskin, A., Piel, F., Tomsche, L., Wisthaler, A., Coggon, M. M., Gkatzelis, G. I., Halliday, H. S.,  
 955 Krechmer, J. E., Moore, R. H., Thomson, D. S., Warneke, C., Wiggins, E. B., and Jimenez, J. L.: Airborne extractive  
 956 electrospray mass spectrometry measurements of the chemical composition of organic aerosol, *Atmos. Meas. Tech.*, 14,  
 957 1545-1559, <https://doi.org/10.5194/amt-14-1545-2021>, 2021.
- 958  
 959 Pechony, O. and Shindell, D. T.: Driving forces of global wildfires over the past millennium and the forthcoming  
 960 century, *P. Natl. Acad. Sci. USA*, 107, 19167, <https://doi.org/10.1073/pnas.1003669107>, 2010.
- 961  
 962 Peng, Q., Palm, B. B., Melander, K. E., Lee, B. H., Hall, S. R., Ullmann, K., Campos, T., Weinheimer, A. J., Apel, E. C.,  
 963 Hornbrook, R. S., Hills, A. J., Montzka, D. D., Flocke, F., Hu, L., Permar, W., Wielgasz, C., Lindaas, J., Pollack, I. B.,  
 964 Fischer, E. V., Bertram, T. H., and Thornton, J. A.: HONO Emissions from Western U.S. Wildfires Provide Dominant  
 965 Radical Source in Fresh Wildfire Smoke, *Environ. Sci. Technol.*, 54, 5954-5963,  
 966 <https://doi.org/10.1021/acs.est.0c00126>, 2020.
- 967  
 968 Permar, W., Wang, Q., Selimovic, V., Wielgasz, C., Yokelson, R. J., Hornbrook, R. S., Hills, A. J., Apel, E. C., Ku, I. T.,  
 969 Zhou, Y., Sive, B. C., Sullivan, A. P., Collett Jr, J. L., Campos, T. L., Palm, B. B., Peng, Q., Thornton, J. A., Garofalo,  
 970 L. A., Farmer, D. K., Kreidenweis, S. M., Levin, E. J. T., DeMott, P. J., Flocke, F., Fischer, E. V., and Hu, L.: Emissions  
 971 of Trace Organic Gases From Western U.S. Wildfires Based on WE-CAN Aircraft Measurements, *J. Geophys. Res.*  
 972 *Atmos.*, 126, e2020JD033838, <https://doi.org/10.1029/2020JD033838>, 2021.
- 973  
 974 Prichard, S. J., O'Neill, S. M., Eagle, P., Andreu, A. G., Drye, B., Dubowy, J., Urbanski, S., and Strand, T. M.: Wildland  
 975 fire emission factors in North America: synthesis of existing data, measurement needs and management applications, *Int.*  
 976 *J. Wildland Fire*, 29, 132-147, <https://doi.org/10.1071/WF19066>, 2020.
- 977  
 978 Reddington, C. L., Spracklen, D. V., Artaxo, P., Ridley, D. A., Rizzo, L. V., and Arana, A.: Analysis of particulate  
 979 emissions from tropical biomass burning using a global aerosol model and long-term surface observations, *Atmos.*  
 980 *Chem. Phys.*, 16, 11083-11106, <https://doi.org/10.5194/acp-16-11083-2016>, 2016.
- 981  
 982 Richter, D., Weibring, P., Walega, J.G., Fried, A., Spuler, S.M., and Taubman, M.S.: Compact highly sensitive multi-  
 983 species airborne mid-IR spectrometer, *Appl. Phys. B.*, <https://doi.org/10.1007/s00340-015-6038-8>, 2015.
- 984  
 985 Rickly, P., Guo, H., Campuzano-Jost, P., Jimenez, J. L., Wolfe, G. M., Bennett, R., Bourgeois, I., Crouse, J. D., Dibb, J.  
 986 E., DiGangi, J. P., Diskin, G. S., Dollner, M., Gargulinski, E. M., Hall, S. R., Halliday, H. S., Hanisco, T. F., Hannun, R.  
 987 A., Liao, J., Moore, R., Nault, B. A., Nowak, J. B., Robinson, C. E., Ryerson, T., Sanchez, K. J., Schöberl, M., Soja, A.  
 988 J., St. Clair, J. M., Thornhill, K. L., Ullmann, K., Wennberg, P. O., Weinzierl, B., Wiggins, E. B., Winstead, E. L., and

- 989 Rollins, A. W.: Emission factors and evolution of SO<sub>2</sub> measured from biomass burning in wild and agricultural fires,  
990 Atmos. Chem. Phys., 2022, 22, 15603-15620, <https://doi.org/10.5194/acp-22-15603-2022>, , 2022.  
991
- 992 Roberts, J. M., Stockwell, C. E., Yokelson, R. J., de Gouw, J., Liu, Y., Selimovic, V., Koss, A. R., Sekimoto, K.,  
993 Coggon, M. M., Yuan, B., Zarzana, K. J., Brown, S. S., Santin, C., Doerr, S. H., and Warneke, C.: The nitrogen budget  
994 of laboratory-simulated western US wildfires during the FIREX 2016 Fire Lab study, Atmos. Chem. Phys., 20, 8807-  
995 8826, <https://doi.org/10.5194/acp-20-8807-2020>, 2020.  
996
- 997 Robinson, M. A., Neuman, J. A., Huey, L. G., Roberts, J. M., Brown, S. S., and Veres, P. R.: Temperature-dependent  
998 sensitivity of iodide chemical ionization mass spectrometers, Atmos. Meas. Tech., 15, 4295-4305,  
999 <https://doi.org/10.5194/amt-15-4295-2022>, 2022.  
1000
- 1001 Robinson, M. A., Decker, Z. C. J., Barsanti, K. C., Coggon, M. M., Flocke, F. M., Franchin, A., Fredrickson, C. D.,  
1002 Gilman, J. B., Gkatzelis, G. I., Holmes, C. D., Lamplugh, A., Lavi, A., Middlebrook, A. M., Montzka, D. M., Palm, B.  
1003 B., Peischl, J., Pierce, B., Schwantes, R. H., Sekimoto, K., Selimovic, V., Tyndall, G. S., Thornton, J. A., Van Rooy, P.,  
1004 Warneke, C., Weinheimer, A. J., and Brown, S. S.: Variability and Time of Day Dependence of Ozone Photochemistry  
1005 in Western Wildfire Plumes, Environ. Sci. Technol., 55, 10280-10290, <https://doi.org/10.1021/acs.est.1c01963>, 2021.  
1006
- 1007 Rollins, A. W., Rickly, P. S., Gao, R. S., Ryerson, T. B., Brown, S. S., Peischl, J., and Bourgeois, I.: Single-photon laser-  
1008 induced fluorescence detection of nitric oxide at sub-parts-per-trillion mixing ratios, Atmos. Meas. Tech., 13, 2425-2439,  
1009 <https://doi.org/10.5194/amt-13-2425-2020>, 2020.  
1010
- 1011 Ryerson, T. B., Williams, E. J., and Fehsenfeld, F. C.: An efficient photolysis system for fast-response NO<sub>2</sub>  
1012 measurements, J. of Geophys. Res.: Atmos., 105, 26447-26461, <https://doi.org/10.1029/2000JD900389>, 2000.  
1013
- 1014 Sachse, G. W., Collins, J., Hill, G. F., Wade, L. O., Burney, L. G., and Ritter, J. A.: Airborne tunable diode laser sensor  
1015 for high-precision concentration and flux measurements of carbon monoxide and methane, Photonics West - Lasers and  
1016 Applications in Science and Engineering, <https://doi.org/10.1117/12.46162>, 1991.  
1017
- 1018 Sachse, S. W., Collins, J. E., Hill, G. F., Wade, L. O., Burney, L. G., and Ritter, J. A.: Airborne tunable diode laser  
1019 sensor for high-precision concentration and flux measurements of carbon monoxide and methane, Proc.SPIE, 1991.  
1020 Schwarz, J. P., Gao, R. S., Spackman, J. R., Watts, L. A., Thomson, D. S., Fahey, D. W., Ryerson, T. B., Peischl, J.,  
1021 Holloway, J. S., Trainer, M., Frost, G. J., Baynard, T., Lack, D. A., de Gouw, J. A., Warneke, C., and Del Negro, L. A.:  
1022 Measurement of the mixing state, mass, and optical size of individual black carbon particles in urban and biomass  
1023 burning emissions, Geophys. Res. Lett., 35, L13810, <https://doi.org/10.1029/2008gl033968>, 2008.  
1024
- 1025 Schneising, O., Buchwitz, M., Reuter, M., Bovensmann, H., and Burrows, J. P.: Severe Californian wildfires in  
1026 November 2018 observed from space: the carbon monoxide perspective, Atmos. Chem. Phys., 20, 3317-3332,  
1027 <https://doi.org/10.5194/acp-20-3317-2020>, 2020.  
1028
- 1029 Schwarz, J. P., Spackman, J. R., Fahey, D. W., Gao, R. S., Lohmann, U., Stier, P., Watts, L. A., Thomson, D. S., Lack,  
1030 D. A., Pfister, L., Mahoney, M. J., Baumgardner, D., Wilson, J. C., and Reeves, J. M.: Coatings and their enhancement  
1031 of black carbon light absorption in the tropical atmosphere, J. Geophys. Res. Atmos., 113, D03203,  
1032 <https://doi.org/10.1029/2007JD009042>, 2008.  
1033
- 1034 Sekimoto, K., Li, S.-M., Yuan, B., Koss, A., Coggon, M., Warneke, C., and de Gouw, J.: Calculation of the sensitivity of  
1035 proton-transfer-reaction mass spectrometry (PTR-MS) for organic trace gases using molecular properties, Int. J. Mass  
1036 Spectrom., 421, 71-94, <https://doi.org/10.1016/j.ijms.2017.04.006>, 2017.  
1037
- 1038 Sekimoto, K., Koss, A. R., Gilman, J. B., Selimovic, V., Coggon, M. M., Zarzana, K. J., Yuan, B., Lerner, B. M., Brown,  
1039 S. S., Warneke, C., Yokelson, R. J., Roberts, J. M., and de Gouw, J.: High- and low-temperature pyrolysis profiles  
1040 describe volatile organic compound emissions from western US wildfire fuels, Atmos. Chem. Phys., 18, 9263-9281,  
1041 <https://doi.org/10.5194/acp-18-9263-2018>, 2018.  
1042
- 1043 Selimovic, V., Yokelson, R. J., Warneke, C., Roberts, J. M., de Gouw, J., Reardon, J., and Griffith, D. W. T.: Aerosol  
1044 optical properties and trace gas emissions by PAX and OP-FTIR for laboratory-simulated western US wildfires during  
1045 FIREX, Atmos. Chem. Phys., 18, 2929-2948, <https://doi.org/10.5194/acp-18-2929-2018>, 2018.  
1046
- 1047 Shrivastava, M., Cappa, C. D., Fan, J., Goldstein, A. H., Guenther, A. B., Jimenez, J. L., Kuang, C., Laskin, A., Martin,  
1048 S. T., Ng, N. L., Petaja, T., Pierce, J. R., Rasch, P. J., Roldin, P., Seinfeld, J. H., Shilling, J., Smith, J. N., Thornton, J. A.,  
1049 Volkamer, R., Wang, J., Worsnop, D. R., Zaveri, R. A., Zelenyuk, A., and Zhang, Q.: Recent advances in understanding

1050 secondary organic aerosol: Implications for global climate forcing, *Rev. Geophys.*, 55, 509-559,  
1051 <https://doi.org/10.1002/2016RG000540>, 2017.

1052

1053 Simpson, I. J., Colman, J. J., Swanson, A. L., Bandy, A. R., Thornton, D. C., Blake, D. R., and Rowland, F. S.: Aircraft  
1054 Measurements of Dimethyl Sulfide (DMS) Using a Whole Air Sampling Technique, *J. Atmos. Chem.*, 39, 191-213,  
1055 <https://doi.org/10.1023/A:1010608529779>, 2001.

1056

1057 Simpson, I. J., Blake, D. R., Blake, N. J., Meinardi, S., Barletta, B., Hughes, S. C., Fleming, L. T., Crawford, J. H.,  
1058 Diskin, G. S., Emmons, L. K., Fried, A., Guo, H., Peterson, D. A., Wisthaler, A., Woo, J.-H., Barré, J., Gaubert, B., Kim,  
1059 J., Kim, M. J., Kim, Y., Knote, C., Mikoviny, T., Pusede, S. E., Schroeder, J. R., Wang, Y., Wennberg, P. O., and Zeng,  
1060 L.: Characterization, sources and reactivity of volatile organic compounds (VOCs) in Seoul and surrounding regions  
1061 during KORUS-AQ, *Elementa: Science of the Anthropocene*, 8, <https://doi.org/10.1525/elementa.434>, 2020.

1062

1063 Spracklen, D. V., Mickley, L. J., Logan, J. A., Hudman, R. C., Yevich, R., Flannigan, M. D., and Westerling, A. L.:  
1064 Impacts of climate change from 2000 to 2050 on wildfire activity and carbonaceous aerosol concentrations in the  
1065 western United States, *J. Geophys. Res. Atmos.*, 114, <https://doi.org/10.1029/2008JD010966>, 2009.

1066

1067 Stark, H., Yatavelli, R. L. N., Thompson, S. L., Kimmel, J. R., Cubison, M. J., Chhabra, P. S., Canagaratna, M. R.,  
1068 Jayne, J. T., Worsnop, D. R., and Jimenez, J. L.: Methods to extract molecular and bulk chemical information from series  
1069 of complex mass spectra with limited mass resolution, *Int. J. Mass Spectrom.*, 389, 26-38,  
1070 <https://doi.org/10.1016/j.ijms.2015.08.011>, 2015.

1071

1072 Stockwell, C. E., Yokelson, R. J., Kreidenweis, S. M., Robinson, A. L., DeMott, P. J., Sullivan, R. C., Reardon, J., Ryan,  
1073 K. C., Griffith, D. W. T., and Stevens, L.: Trace gas emissions from combustion of peat, crop residue, domestic biofuels,  
1074 grasses, and other fuels: configuration and Fourier transform infrared (FTIR) component of the fourth Fire Lab at  
1075 Missoula Experiment (FLAME-4), *Atmos. Chem. Phys.*, 14, 9727-9754, <https://doi.org/10.5194/acp-14-9727-2014>,  
1076 2014.

1077

1078 Stockwell, C. E., Veres, P. R., Williams, J., and Yokelson, R. J.: Characterization of biomass burning emissions from  
1079 cooking fires, peat, crop residue, and other fuels with high-resolution proton-transfer-reaction time-of-flight mass  
1080 spectrometry, *Atmos. Chem. Phys.*, 15, 845-865, <https://doi.org/10.5194/acp-15-845-2015>, 2015.

1081

1082 Stockwell, C. E., Jayarathne, T., Cochrane, M. A., Ryan, K. C., Putra, E. I., Saharjo, B. H., Nurhayati, A. D., Albar, I.,  
1083 Blake, D. R., Simpson, I. J., Stone, E. A., and Yokelson, R. J.: Field measurements of trace gases and aerosols emitted by  
1084 peat fires in Central Kalimantan, Indonesia, during the 2015 El Niño, *Atmos. Chem. Phys.*, 16, 11711-11732,  
1085 <https://doi.org/10.5194/acp-16-11711-2016>, 2016.

1086

1087 Stönnner, C., Derstroff, B., Klüpfel, T., Crowley, J. N., and Williams, J.: Glyoxal measurement with a proton transfer  
1088 reaction time of flight mass spectrometer (PTR-TOF-MS): characterization and calibration, *J. Mass Spectrom.*, 52, 30-  
1089 35, <https://doi.org/10.1002/jms.3893>, 2017.

1090

1091 Sudo, K. and Akimoto, H.: Global source attribution of tropospheric ozone: Long-range transport from various source  
1092 regions, *J. Geophys. Res. Atmos.*, 112, <https://doi.org/10.1029/2006JD007992>, 2007.

1093

1094 Theys, N., Volkamer, R., Müller, J. F., Zarzana, K. J., Kille, N., Clarisse, L., De Smedt, I., Lerot, C., Finkenzeller, H.,  
1095 Hendrick, F., Koenig, T. K., Lee, C. F., Knote, C., Yu, H., and Van Roozendael, M.: Global nitrous acid emissions and  
1096 levels of regional oxidants enhanced by wildfires, *Nat. Geosci.*, 13, 681-686, <https://doi.org/10.1038/s41561-020-0637-7>,  
1097 2020.

1098

1099 Tomsche, L., Piel, F., Mikoviny, T., Nielsen, C. J., Guo, H., Campuzano-Jost, P., Nault, B. A., Schueneman, M. K.,  
1100 Jimenez, J. L., Halliday, H., Diskin, G., DiGangi, J. P., Nowak, J. B., Wiggins, E. B., Gargulinski, E., Soja, A. J., and  
1101 Wisthaler, A.: Measurement report: Emission factors of NH<sub>3</sub> and NH<sub>x</sub> for wildfires and agricultural fires in the United  
1102 States, *Atmos. Chem. Phys.*, 23, 2331-2343, <https://doi.org/10.5194/acp-23-2331-2023>, 2023.

1103

1104 Thornhill, G. D., Ryder, C. L., Highwood, E. J., Shaffrey, L. C., and Johnson, B. T.: The effect of South American  
1105 biomass burning aerosol emissions on the regional climate, *Atmos. Chem. Phys.*, 18, 5321-5342,  
1106 <https://doi.org/10.5194/acp-18-5321-2018>, 2018.

1107

1108 Tian, H., Lu, C., Ciais, P., Michalak, A. M., Canadell, J. G., Saikawa, E., Huntzinger, D. N., Gurney, K. R., Sitch, S.,  
1109 Zhang, B., Yang, J., Bousquet, P., Bruhwiler, L., Chen, G., Dlugokencky, E., Friedlingstein, P., Melillo, J., Pan, S.,

- 1110 Poulter, B., Prinn, R., Saunio, M., Schwalm, C. R., and Wofsy, S. C.: The terrestrial biosphere as a net source of  
1111 greenhouse gases to the atmosphere, *Nature*, 531, 225-228, <https://doi.org/10.1038/nature16946>, 2016.  
1112
- 1113 Tsimpidi, A. P., Karydis, V. A., Pandis, S. N., and Lelieveld, J.: Global-scale combustion sources of organic aerosols:  
1114 sensitivity to formation and removal mechanisms, *Atmos. Chem. Phys.*, 17, 7345-7364, [https://doi.org/10.5194/acp-17-](https://doi.org/10.5194/acp-17-7345-2017)  
1115 [7345-2017](https://doi.org/10.5194/acp-17-7345-2017), 2017.  
1116
- 1117 Urbanski, S. P., Hao, W. M. and Baker, S.: Chapter 4 Chemical Composition of Wildland Fire Emissions, *Dev. Environ.*  
1118 *Sci.*, 8, 79-107, [https://doi.org/10.1016/S1474-8177\(08\)00004-1](https://doi.org/10.1016/S1474-8177(08)00004-1), 2008.  
1119
- 1120 Vasilkov, A., Krotkov, N., Yang, E. S., Lamsal, L., Joiner, J., Castellanos, P., Fasnacht, Z., and Spurr, R.: Explicit and  
1121 consistent aerosol correction for visible wavelength satellite cloud and nitrogen dioxide retrievals based on optical  
1122 properties from a global aerosol analysis, *Atmos. Meas. Tech.*, 14, 2857-2871, [https://doi.org/10.5194/amt-14-2857-](https://doi.org/10.5194/amt-14-2857-2021)  
1123 [2021](https://doi.org/10.5194/amt-14-2857-2021), 2021.  
1124
- 1125 Vay, S. A., Tyler, S. C., Choi, Y., Blake, D. R., Blake, N. J., Sachse, G. W., Diskin, G. S., and Singh, H. B.: Sources and  
1126 transport of  $\Delta^{14}\text{C}$  in  $\text{CO}_2$  within the Mexico City Basin and vicinity, *Atmos. Chem. Phys.*, 9, 4973-4985,  
1127 <https://doi.org/10.5194/acp-9-4973-2009>, 2009.  
1128
- 1129 Veres, P. R., Neuman, J. A., Bertram, T. H., Assaf, E., Wolfe, G. M., Williamson, C. J., Weinzierl, B., Tilmes, S.,  
1130 Thompson, C. R., Thames, A. B., Schroder, J. C., Saiz-Lopez, A., Rollins, A. W., Roberts, J. M., Price, D., Peischl, J.,  
1131 Nault, B. A., Møller, K. H., Miller, D. O., Meinardi, S., Li, Q., Lamarque, J.-F., Kupc, A., Kjaergaard, H. G., Kinnison,  
1132 D., Jimenez, J. L., Jernigan, C. M., Hornbrook, R. S., Hills, A., Dollner, M., Day, D. A., Cuevas, C. A., Campuzano-Jost,  
1133 P., Burkholder, J., Bui, T. P., Brune, W. H., Brown, S. S., Brock, C. A., Bourgeois, I., Blake, D. R., Apel, E. C., and  
1134 Ryerson, T. B.: Global airborne sampling reveals a previously unobserved dimethyl sulfide oxidation mechanism in the  
1135 marine atmosphere, *P. Natl. Acad. Sci.*, 117, 4505, <https://doi.org/10.1073/pnas.1919344117>, 2020.  
1136
- 1137 Wang, S., Coggon, M. M., Gkatzelis, G. I., Warneke, C., Bourgeois, I., Ryerson, T. B., Peischl, J., Veres, P. R., Neuman,  
1138 J. A., Hair, J., Shingler, T., Fenn, M., Diskin, G., Huey, L. G., Lee, Y. R., Apel, E. C., Hornbrook, R. S., Hills, A. J.,  
1139 Hall, S. R., Ullmann, K., Bela, M. M., Trainer, M. K., Kumar, R., Orlando, J. J., Flocke, F. M., and Emmons, L. K.:  
1140 Chemical Tomography in a Fresh Wildland Fire Plume: a Large Eddy Simulation (LES) Study, *J. Geophys. Res. Atmos.*,  
1141 126, e2021JD035203, <https://doi.org/10.1029/2021JD035203>, 2021.  
1142
- 1143 Ward, D. S., Kloster, S., Mahowald, N. M., Rogers, B. M., Randerson, J. T., and Hess, P. G.: The changing radiative  
1144 forcing of fires: global model estimates for past, present and future, *Atmos. Chem. Phys.*, 12, 10857-10886,  
1145 <https://doi.org/10.5194/acp-12-10857-2012>, 2012.  
1146
- 1147 Warneke, C., Roberts, J. M., Veres, P., Gilman, J., Kuster, W. C., Burling, I., Yokelson, R., and de Gouw, J. A.: VOC  
1148 identification and inter-comparison from laboratory biomass burning using PTR-MS and PIT-MS, *Int. J. Mass*  
1149 *Spectrom.*, 303, 6-14, <https://doi.org/10.1016/j.ijms.2010.12.002>, 2011.  
1150
- 1151 Warneke, C., Schwarz, J. P., Dibb, J., Kalashnikova, O., Frost, G., Al-Saad, J., Brown, S. S., Brewer, W. A., Soja, A.,  
1152 Seidel, F. C., Washenfelder, R. A., Wiggins, E. B., Moore, R. H., Anderson, B. E., Jordan, C., Yacovitch, T. I., Herndon,  
1153 S. C., Liu, S., Kuwayama, T., Jaffe, D., Johnston, N., Selimovic, V., Yokelson, R., Giles, D. M., Holben, B. N., Goloub,  
1154 P., Popovici, I., Trainer, M., Kumar, A., Pierce, R. B., Fahey, D., Roberts, J., Gargulinski, E. M., Peterson, D. A., Ye, X.,  
1155 Thapa, L. H., Saide, P. E., Fite, C. H., Holmes, C. D., Wang, S., Coggon, M. M., Decker, Z. C. J., Stockwell, C. E., Xu,  
1156 L., Gkatzelis, G., Aikin, K., Lefer, B., Kaspari, J., Griffin, D., Zeng, L., Weber, R., Hastings, M., Chai, J., Wolfe, G. M.,  
1157 Hanisco, T. F., Liao, J., Campuzano Jost, P., Guo, H., Jimenez, J. L., Crawford, J., and The, F.-A. Q. S. T.: Fire  
1158 Influence on Regional to Global Environments and Air Quality (FIREX-AQ), *J. of Geophys. Res.: Atmos.*, 128,  
1159 e2022JD037758, <https://doi.org/10.1029/2022JD037758>, 2023.  
1160
- 1161 Weibring, P., Richter, D., Walega, J. G., and Fried, A.: First demonstration of a high performance difference frequency  
1162 spectrometer on airborne platforms, *Opt. Express*, 15, 13476-13495, <https://doi.org/10.1364/OE.15.013476>, 2007.  
1163
- 1164 Westerling, A. L., Hidalgo, H. G., Cayan, D. R., and Swetnam, T. W.: Warming and Earlier Spring Increase Western  
1165 U.S. Forest Wildfire Activity, *Science*, 313, 940, <https://doi.org/10.1126/science.1128834>, 2006.  
1166
- 1167 Wiedinmyer, C. and Hurteau, M. D.: Prescribed Fire As a Means of Reducing Forest Carbon Emissions in the Western  
1168 United States, *Environ. Sci. Technol.*, 44, 1926-1932, <https://doi.org/10.1021/es902455e>, 2010.  
1169

1170 Wiedinmyer, C., Akagi, S. K., Yokelson, R. J., Emmons, L. K., Al-Saadi, J. A., Orlando, J. J., and Soja, A. J.: The Fire  
1171 INventory from NCAR (FINN): a high resolution global model to estimate the emissions from open burning, *Geosci.*  
1172 *Model Dev.*, 4, 625-641, <https://doi.org/10.5194/gmd-4-625-2011>, 2011.

1173  
1174 Wiggins, E. B., Soja, A. J., Gargulinski, E., Halliday, H. S., Pierce, R. B., Schmidt, C. C., Nowak, J. B., DiGangi, J. P.,  
1175 Diskin, G. S., Katich, J. M., Perring, A. E., Schwarz, J. P., Anderson, B. E., Chen, G., Crosbie, E. C., Jordan, C.,  
1176 Robinson, C. E., Sanchez, K. J., Shingler, T. J., Shook, M., Thornhill, K. L., Winstead, E. L., Ziemba, L. D., and Moore,  
1177 R. H.: High Temporal Resolution Satellite Observations of Fire Radiative Power Reveal Link Between Fire Behavior  
1178 and Aerosol and Gas Emissions, *Geophys. Res. Lett.*, 47, e2020GL090707, <https://doi.org/10.1029/2020GL090707>,  
1179 2020.

1180  
1181 Wolfe, G. M., Hanisco, T. F., Arkinson, H. L., Blake, D. R., Wisthaler, A., Mikoviny, T., Ryerson, T. B., Pollack, I.,  
1182 Peischl, J., Wennberg, P. O., Crounse, J. D., St. Clair, J. M., Teng, A., Huey, L. G., Liu, X., Fried, A., Weibring, P.,  
1183 Richter, D., Walega, J., Hall, S. R., Ullmann, K., Jimenez, J. L., Campuzano-Jost, P., Bui, T. P., Diskin, G., Podolske, J.  
1184 R., Sachse, G., and Cohen, R. C.: Photochemical evolution of the 2013 California Rim Fire: synergistic impacts of  
1185 reactive hydrocarbons and enhanced oxidants, *Atmos. Chem. Phys.*, 22, 4253-4275, [https://doi.org/10.5194/acp-22-](https://doi.org/10.5194/acp-22-4253-2022)  
1186 [4253-2022](https://doi.org/10.5194/acp-22-4253-2022), 2022.

1187  
1188 Xu, L., Crounse, J. D., Vasquez, K., T., Allen, H., Wennberg, P. O., Bourgeois, I., Brown, S. S., Campuzano-Jost, P.,  
1189 Coggon, M. M., Crawford, J. H., DiGangi J. P., Diskin, G. S., Fried, A., Gargulinski, E. M., Gilman, J. B., Gkatzelis, G.  
1190 I., Guo, H., Hair, J. W., Hall, S. R., Halliday, H. A., Hanisco, T. F., Hannun, R. A., Holmes, C. D., Huey, L. G., Jimenez,  
1191 J. L., Lamplugh, A., Lee, Y. R., Liao, J., Lindaas, J., Neuman, J. A., Nowak, J. B., Peischl, J., Peterson, D. A., Piel, F.,  
1192 Richter, D., Rickly, P. S., Robinson, M. A., Rollins, A. W., Ryerson, T. B., Sekimoto, K., Selimovic, V., Shingler, T.,  
1193 Soja, A. J., St. Clair, J. M., Tanner, D. J., Ullmann, K., Veres P. R., Walega, J., Warneke, C., Washenfelder, R. A.,  
1194 Weibring, P., Wisthaler, A., Wolfe, G. M., Womack, C. C., and Yokelson, R. J.: Ozone chemistry in western U.S.  
1195 wildfire plumes, *Sci. Adv.*, 7, eabl3648, <https://doi.org/10.1126/sciadv.abl3648>, 2021.

1196  
1197 van der Velde, I. R., van der Werf, G. R., Houweling, S., Eskes, H. J., Veeffkind, J. P., Borsdorff, T., and Aben, I.:  
1198 Biomass burning combustion efficiency observed from space using measurements of CO and NO<sub>2</sub> by the  
1199 TROPOspheric Monitoring Instrument (TROPOMI), *Atmos. Chem. Phys.*, 21, 597-616, [https://doi.org/10.5194/acp-21-](https://doi.org/10.5194/acp-21-597-2021)  
1200 [597-2021](https://doi.org/10.5194/acp-21-597-2021), 2021.

1201  
1202 Yokelson, R. J., Griffith, D. W. T., and Ward, D. E.: Open-path Fourier transform infrared studies of large-scale  
1203 laboratory biomass fires, *J. Geophys. Res. Atmos.*, 101, 21067-21080, <https://doi.org/10.1029/96JD01800>, 1996.

1204  
1205 Yokelson, R. J., Christian, T. J., Karl, T. G., and Guenther, A.: The tropical forest and fire emissions experiment:  
1206 laboratory fire measurements and synthesis of campaign data, *Atmos. Chem. Phys.*, 8, 3509-3527,  
1207 <https://doi.org/10.5194/acp-8-3509-2008>, 2008.

1208  
1209 Yokelson, R. J., Burling, I. R., Gilman, J. B., Warneke, C., Stockwell, C. E., de Gouw, J., Akagi, S. K., Urbanski, S. P.,  
1210 Veres, P., Roberts, J. M., Kuster, W. C., Reardon, J., Griffith, D. W. T., Johnson, T. J., Hosseini, S., Miller, J. W.,  
1211 Cocker Iii, D. R., Jung, H., and Weise, D. R.: Coupling field and laboratory measurements to estimate the emission  
1212 factors of identified and unidentified trace gases for prescribed fires, *Atmos. Chem. Phys.*, 13, 89-116,  
1213 <https://doi.org/10.5194/acp-13-89-2013>, 2013.

1214  
1215 Yuan, B., Koss, A., Warneke, C., Gilman, J. B., Lerner, B. M., Stark, H., and de Gouw, J. A.: A high-resolution time-of-  
1216 flight chemical ionization mass spectrometer utilizing hydronium ions (H<sub>3</sub>O<sup>+</sup> ToF-CIMS) for measurements of volatile  
1217 organic compounds in the atmosphere, *Atmos. Meas. Tech.*, 9, 2735-2752, <https://doi.org/10.5194/amt-9-2735-2016>,  
1218 2016.

1219  
1220 Yue, C., Ciais, P., Cadule, P., Thonicke, K., and van Leeuwen, T. T.: Modelling the role of fires in the terrestrial carbon  
1221 balance by incorporating SPITFIRE into the global vegetation model ORCHIDEE – Part 2: Carbon emissions and the  
1222 role of fires in the global carbon balance, *Geosci. Model Dev.*, 8, 1321-1338, <https://doi.org/10.5194/gmd-8-1321-2015>,  
1223 2015.

1224  
1225 Zarzana, K. J., Selimovic, V., Koss, A. R., Sekimoto, K., Coggon, M. M., Yuan, B., Dubé, W. P., Yokelson, R. J.,  
1226 Warneke, C., de Gouw, J. A., Roberts, J. M., and Brown, S. S.: Primary emissions of glyoxal and methylglyoxal from  
1227 laboratory measurements of open biomass burning, *Atmos. Chem. Phys.*, 18, 15451-15470, [https://doi.org/10.5194/acp-](https://doi.org/10.5194/acp-18-15451-2018)  
1228 [18-15451-2018](https://doi.org/10.5194/acp-18-15451-2018), 2018.

1229

1230 Zhao, X. and Wang, L.: Atmospheric Oxidation Mechanism of Furfural Initiated by Hydroxyl Radicals, The Journal of  
1231 Physical Chemistry A, 121, 3247-3253, <https://doi.org/10.1021/acs.jpca.7b00506>, 2017.  
1232  
1233 Zheng, W., Flocke, F. M., Tyndall, G. S., Swanson, A., Orlando, J. J., Roberts, J. M., Huey, L. G., and Tanner, D. J.:  
1234 Characterization of a thermal decomposition chemical ionization mass spectrometer for the measurement of peroxy acyl  
1235 nitrates (PANs) in the atmosphere, Atmos. Chem. Phys., 11, 6529-6547, <https://doi.org/10.5194/acp-11-6529-2011>,  
1236 2011.